Research Square

Preprints are preliminary reports that have not undergone peer review.
They should not be considered conclusive, used to inform clinical practice,
or referenced by the media as validated information.

Coupling advanced earth observation, Machine learning, GeoAI, and CA-ANN model for assessing Spatio-temporal LULC change in Gilgel Gibe I Watershed, Upper Omo-Gibe Basin, Ethiopia

Ermiyas Asfaw Molla

ermiyas.asfaw@amu.edu.et

Arba Minch Water Technology Institute, Arba Minch University

Amanuel Tesfaye Kebebew

Arba Minch Water Technology Institute, Arba Minch University

Albeza Asfaw Molla

Arba Minch Water Technology Institute, Arba Minch University

Tilahun Kasa Weldetsadik

Arba Minch Water Technology Institute, Arba Minch University

Zelalem Abera Angello

Arba Minch Water Technology Institute, Arba Minch University

Sintayehu Yadeta Tolla

Arba Minch Water Technology Institute, Arba Minch University

Robel Fikadu Alemayehu

University of Idaho

Brook Legese Dadhe

Indian Institute of Technology Roorkee

Nahom Bekele Mena

The Hong Kong Polytechnic University

Research Article

Keywords: LULC change, Google Earth Engine, GeoAI, CA-ANN, Machine learning, Transition probability, Gilgel Gibe I Watershed

Posted Date: September 4th, 2026

DOI: https://doi.org/10.21203/rs.3.rs-10678132/v1

License: This work is licensed under a Creative Commons Attribution 4.0 International License.
Read Full License

Additional Declarations: No competing interests reported.

Coupling advanced earth observation, Machine learning, GeoAI, and CA-ANN model for assessing Spatio-temporal LULC change in Gilgel Gibe I Watershed, Upper Omo-Gibe Basin, Ethiopia.

Ermiyas Asfaw Molla[1*], Amanuel Tesfaye Kebebew[2], Albeza Asfaw Molla[2], Tilahun Kassa Weldetsadik[1], Zelalem Abera Angello[1], Sintayehu Yadeta Tolla[1], Robel Fikadu Alemayehu[3], Brook Legese Dadhe[4], Nahom Bekele Mena[5],

1 Faculty of water supply and environmental engineering, Arba Minch Water Technology Institute, Arba Minch University, Arba Minch, Ethiopia

2 Faculty of Hydraulic and water resource engineering, Arba Minch Water Technology Institute, Arba Minch University, Arba Minch, Ethiopia

3 University of Idaho, Moscow, United States

4 Department of Water Resources Development and Management, Indian Institute of Technology Roorkee, Roorkee, India

5 Faculty of construction and environment, Department of Land Surveying and Geo-Informatics, The Hong Kong Polytechnic University, Hung Hom, Hong Kong

*Correspondence: ermiyas.asfaw@amu.edu.et

Abstract

Land use and land cover (LULC) change represents one of the most significant manifestations of human-environment interactions and a primary driver of global environmental change. Rapid LULC transformation in the Gibe I Watershed has created substantial challenges for ecosystem service provisioning, biodiversity conservation, and sustainable development. Although LULC change prediction using geospatial artificial intelligence (GeoAI) and multi-factor transition potential modelling has received increasing attention, studies integrating these approaches in the Omo-Gibe basin of Ethiopia remain limited. This study integrates cloud-based remote sensing classification with a Cellular Automata-Artificial Neural Network (CA-ANN) geospatial model to comprehensively assess historical, contemporary, and projected LULC dynamics in the Gibe I Watershed. Multi-temporal Landsat and Sentinel-2 imagery were processed through Google Earth Engine using Random Forest supervised classification to generate high-accuracy LULC maps for 2004, 2014, and 2024, achieving overall classification accuracies of 88.45%, 90.62%, and 93.8% respectively, and with substantial Kappa coefficients exceeding 0.89 in these years. Transition potential modeling revealed pronounced Spatio-temporal transformations, with built-up and agricultural areas expanding substantially at the expense of forest, grassland, and bare land. Forest cover declined by 49,851.53 hectares (58.15%) between 2004 and 2024, while agricultural land increased by 83,219.68 hectares (32.25%) during the same period. The CA-ANN model incorporated six driving factors including elevation, slope, and proximity variables—and was validated against 2024 LULC classifications before projecting future scenarios for 2034 and 2044. Projections indicate continued land transformation, with built-up areas expanding further while forest and grassland areas decline progressively. These LULC changes have profound implications for ecohydrological regimes and threaten ecosystem services, livelihoods, and environmental sustainability. The findings provide critical decision-support tools for land use planning, water resource management, and environmental conservation in rapidly transforming tropical watersheds.

Keywords: LULC change; Google Earth Engine; GeoAI, CA-ANN; Machine learning; Transition probability; Gilgel Gibe I Watershed

1 Introduction

Land use and land cover (LULC) change represents one of the most significant manifestations of human-environment interactions (Khan & Chen, 2025), serving as a primary driver of global environmental change with profound implications for ecosystem services (Fagun et al., 2025; Kusiima et al., 2022; Makwinja et al., 2021), biodiversity conservation (Baidoo et al., 2023), and sustainable development (Mafiana et al., 2025; W. Mekuria et al., 2021). The accelerating pace of LULC transformation, driven by anthropogenic activities including agricultural expansion, urbanization, and infrastructure development, has fundamentally altered terrestrial landscapes across multiple spatial and temporal scales (Brunori et al., 2017; Sitati et al., 2024). In developing countries, particularly within Sub-Saharan Africa, rapid population growth and socioeconomic development have intensified land conversion pressures, resulting in substantial losses of natural vegetation and agricultural productivity (Bosma & Hein, 2023; D. Tilahun et al., 2022). Understanding the spatiotemporal patterns of these changes and projecting future trajectories has become critical for achieving sustainable land management and addressing global challenges such as food security, climate change mitigation, and ecosystem integrity preservation (Kariuki et al., 2021; Makwinja et al., 2021).

The advent of advanced remote sensing technologies and geospatial analytical tools has revolutionized the capacity to monitor and assess LULC changes at unprecedented spatial resolutions and temporal frequencies (Dubertret et al., 2022; Midekisa et al., 2017; Yang et al., 2022). Landsat satellite missions, providing continuous Earth observation data since 1972, have established an invaluable archive for long-term LULC change detection studies(Gorelick et al., 2017; Shimizu et al., 2023; Wulder et al., 2019). The paradigm shift toward cloud-based geospatial processing platforms, particularly Google Earth Engine (GEE), has democratized access to vast repositories of remotely sensed imagery and computational resources, facilitating large-scale LULC classification and change analysis (Kumar & Mutanga, 2018; Midekisa et al., 2017; Yang et al., 2022). Recent studies have demonstrated the effectiveness of GEE-based approaches for LULC monitoring across diverse geographical contexts, with classification accuracies frequently exceeding 90% (Aldiansyah & Saputra, 2022; Dubertret et al., 2022; Feng et al., 2022; Jamei et al., 2022). Comparative analyses have shown that Random Forest (RF) consistently outperforms other machine learning algorithms including Support Vector Machine (SVM) and Classification and Regression Trees (CART) for LULC classification, achieving overall accuracies of 91-99% with Kappa coefficients between 0.85-0.99 (Raguraman & Bhardwaj, 2024; Talukdar et al., 2020). The synergy between cloud computing platforms and advanced classification algorithms has enabled researchers to overcome traditional computational limitations and conduct analyses at watershed, regional, and even continental scales (Dubertret et al., 2022; Feng et al., 2022; Midekisa et al., 2017; Tamiminia et al., 2020).

With the emergence of GeoAI science and tools, the prediction and simulation of future LULC changes have emerged as critical components of proactive environmental planning and sustainable land management strategies(Deressu et al. 2025; Hosseini, Atazadeh, and Rajabifard 2025) . Among various GeoAI based modelling

approaches, the integration of Cellular Automata (CA) Artificial Neural Network (ANN) models has gained substantial traction due to its capability to simulate complex spatial patterns and temporal transitions in land cover (Baig et al., 2022; Islam et al., 2023). The CA-ANN model combines the temporal prediction power of Markov chains, which capture land use transition probabilities, with the spatial dynamics modeling capability of cellular automata and the pattern recognition strength of artificial neural networks (Lukas et al., 2023; Thakur et al., 2026). This hybrid approach has been successfully implemented across diverse geographical contexts, achieving validation accuracies ranging from 79% to 95% with Kappa coefficients typically exceeding 0.75 (Baig et al., 2022; Blissag et al., 2024; Değermenci, 2023; Lukas et al., 2023). Studies employing CA-ANN models through platforms such as the MOLUSCE plugin in QGIS have shown particular effectiveness in simulating urban expansion, agricultural land conversion, and vegetation cover changes (Fontana et al. 2023; Muhammad et al. 2022; Tilahun, Gashu, and Shiferaw 2022; Xu, Zhou, and Li 2022).

Ethiopia, particularly the Omo-Gibe River Basin, has experienced substantial LULC transformations over recent decades, driven by rapid population growth, agricultural intensification, and infrastructure development (A. Aneseyee et al., 2019; Derebe et al., 2022; Lukas et al., 2023). The Gibe I Watershed, a strategically important sub-basin within the Omo-Gibe system, has undergone notable land transformation characterized by expansion of cultivated areas and settlements at the expense of natural vegetation and forest cover (Dagnachew et al., 2020; Derebe et al., 2022). These changes have significant implications for watershed hydrology, soil erosion rates, sediment yield, and reservoir sedimentation, potentially threatening long-term sustainability of hydropower generation and water resource availability. Previous studies in the Omo-Gibe Basin have documented dramatic increases in agricultural land by 63% and built-up areas by substantial margins, accompanied by forest cover losses exceeding 48% over multi-decadal periods (A. Aneseyee et al., 2019; Derebe et al., 2022) . Such rapid LULC transformations have been linked to increased surface runoff, reduced groundwater recharge, elevated erosion rates, and heightened vulnerability to flooding and drought events (A. Aneseyee et al., 2019; Demessie et al., 2025; Pereira et al., 2022) .

Although geospatial machine-learning have been widely applied for LULC mapping, integrated assessments combining historical land-cover dynamics with future spatial simulations remain limited for the Upper Gibe Watershed. This study addresses this gap by applying an established GEE–RF–CA–ANN framework to generate consistent historical classifications and future land-use projections to support sustainable watershed management. Therefore, this study applies an integrated GEE–RF–CA–ANN framework to comprehensively assess past, present, and future LULC dynamics in the Gibe I Watershed, Ethiopia. Specifically, the research objectives are to: (1) generate high-accuracy LULC maps for 2004, 2014, and 2024 using Random Forest supervised classification within Google Earth Engine and evaluate classification performance using confusion matrix-based accuracy metrics; (2) analyze spatiotemporal LULC change patterns and quantify land conversion dynamics across the three time periods; (3) implement and validate a CA-ANN model using the MOLUSCE plugin in QGIS, incorporating multiple driving factors including topographic, proximity, and socioeconomic variables; and (4) simulate future LULC scenarios for 2034 and 2044 to project potential land transformation trajectories under current trends. The primary contribution of this study is the application of an integrated GEE–RF–CA–ANN framework to generate a consistent assessment of historical (2004–2024) and projected (2034 and 2044) LULC dynamics for the Upper Gibe Watershed. By combining cloud-based image processing, machine-learning

classification, and spatial simulation, the study provides updated spatial evidence to support watershed management and regional land-use planning in an area where comprehensive long-term predictive assessments remain limited.

2 Materials and methods

2.1 Study area

The Gibe I watershed is situated in the central-southwestern part of Ethiopia within the Omo-Gibe River Basin, spanning approximately 7°00'–8°20'N latitude and 36°40'–37°20'E longitude. The Watershed delineation through ArcGIS 10.8 at downstream of Gilgel Gibe I Dam outlet covers area of 4332Km^2. The watershed encompasses diverse topography ranging from highlands to mid-slopes and lowland plains, with elevations varying from approximately 1,000 to 2,800 meters above sea level. This region experiences a sub-humid to humid tropical climate with a unimodal rainfall regime concentrated during the June-September rainy season, with mean annual precipitation often exceeding 1,200 mm (Z. A. Tilahun et al., 2023). The watershed is hydrologically dominated by the Gibe River network, which is the main river of the watershed supporting vital water resources for irrigation, hydropower generation, and domestic use, contributing significantly to the downstream ecological integrity of the Omo-Turkana system(Fanta et al., 2022; Orkodjo et al., 2022).

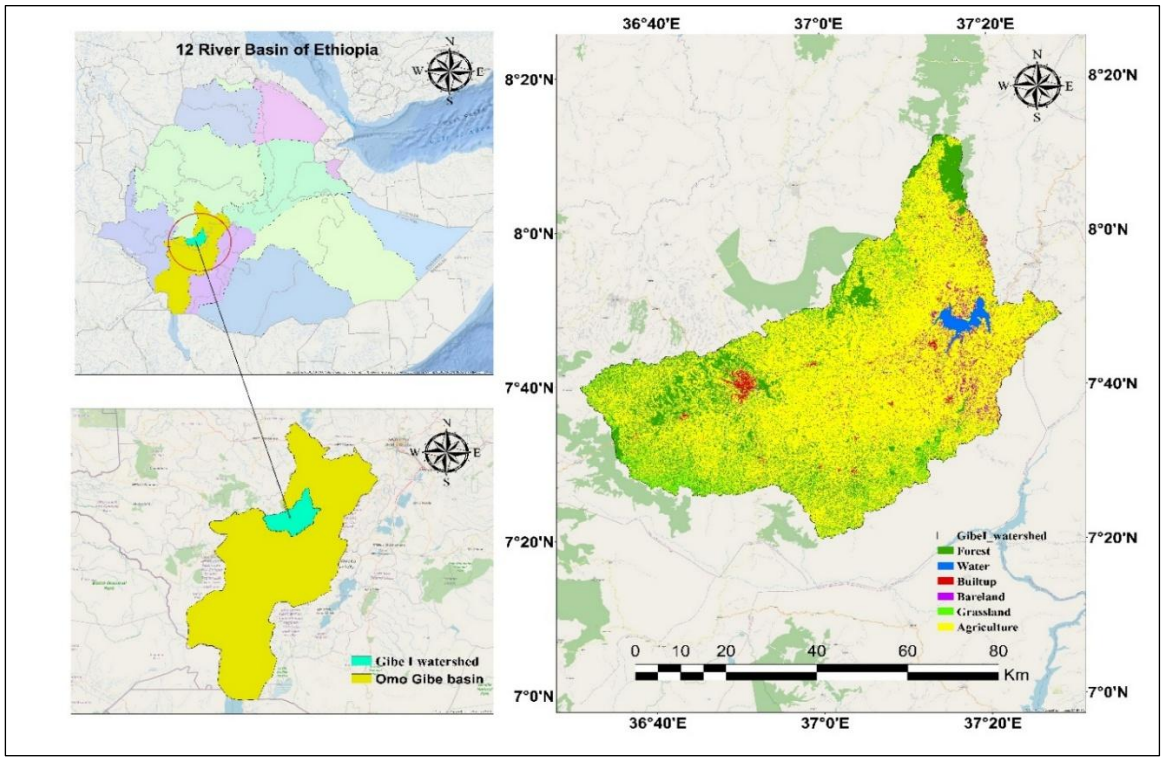


Figure 1 study area

Predominant land cover comprises agricultural land, forest patches, grassland, water bodies, built-up areas, and bare surfaces, reflecting extensive rain-fed agriculture and expanding rural settlements that underpin the local economy. The region has experienced notable landscape transformation characterized by deforestation and conversion of natural forests and shrublands to cropland, largely driven by population growth, agricultural expansion, and infrastructure development (Z. A. Tilahun et al., 2024). These pronounced socio-ecological

pressures and documented landscape changes make the Gibe I watershed a representative and scientifically pertinent case for assessing past, present, and future LULC dynamics using integrated Earth observation and machine-learning-enabled geospatial prediction approaches.

2.2 Google Earth Engine Platform

Google Earth Engine (GEE) was employed as the primary cloud-based geospatial processing platform for LULC classification and change detection analysis. GEE provides access to petabyte-scale satellite imagery archives and computational resources, enabling efficient processing of large-scale multi-temporal datasets without requiring extensive local computing infrastructure(Alshehri et al., 2025; Tamiminia et al., 2020). The platform's cloud-based architecture facilitates rapid analysis of Landsat and Sentinel time-series imagery through its built-in JavaScript API and integrated machine learning algorithms (Yang et al., 2022). For this study, GEE was utilized to acquire, pre-process, and classify multi-temporal satellite imagery spanning 2004 to 2024 through automated workflows. The platform's capability to process vast amounts of remote sensing data and apply advanced classification algorithms makes it particularly suitable for watershed-scale LULC change detection studies in data-scarce regions like Ethiopia.

2.3 Research methodology

This study employed an integrated Earth observation and geospatial modeling framework, as illustrated in Fig. 2, combining cloud-based remote sensing analysis and spatially explicit prediction. Multi-temporal Landsat (ETM+, OLI/TIRS) and Sentinel-2 MSI imagery were processed in Google Earth Engine for index computation, preprocessing, and Random Forest–based supervised classification to generate LULC maps for 2004, 2014, and 2024, followed by accuracy assessment using confusion matrix metrics. Change detection outputs and standardized driving factors were subsequently incorporated into the MOLUSCE plugin in QGIS to model transition potentials using a CA–ANN approach, which was validated against observed 2024 LULC before simulating future scenarios for 2034 and 2044.

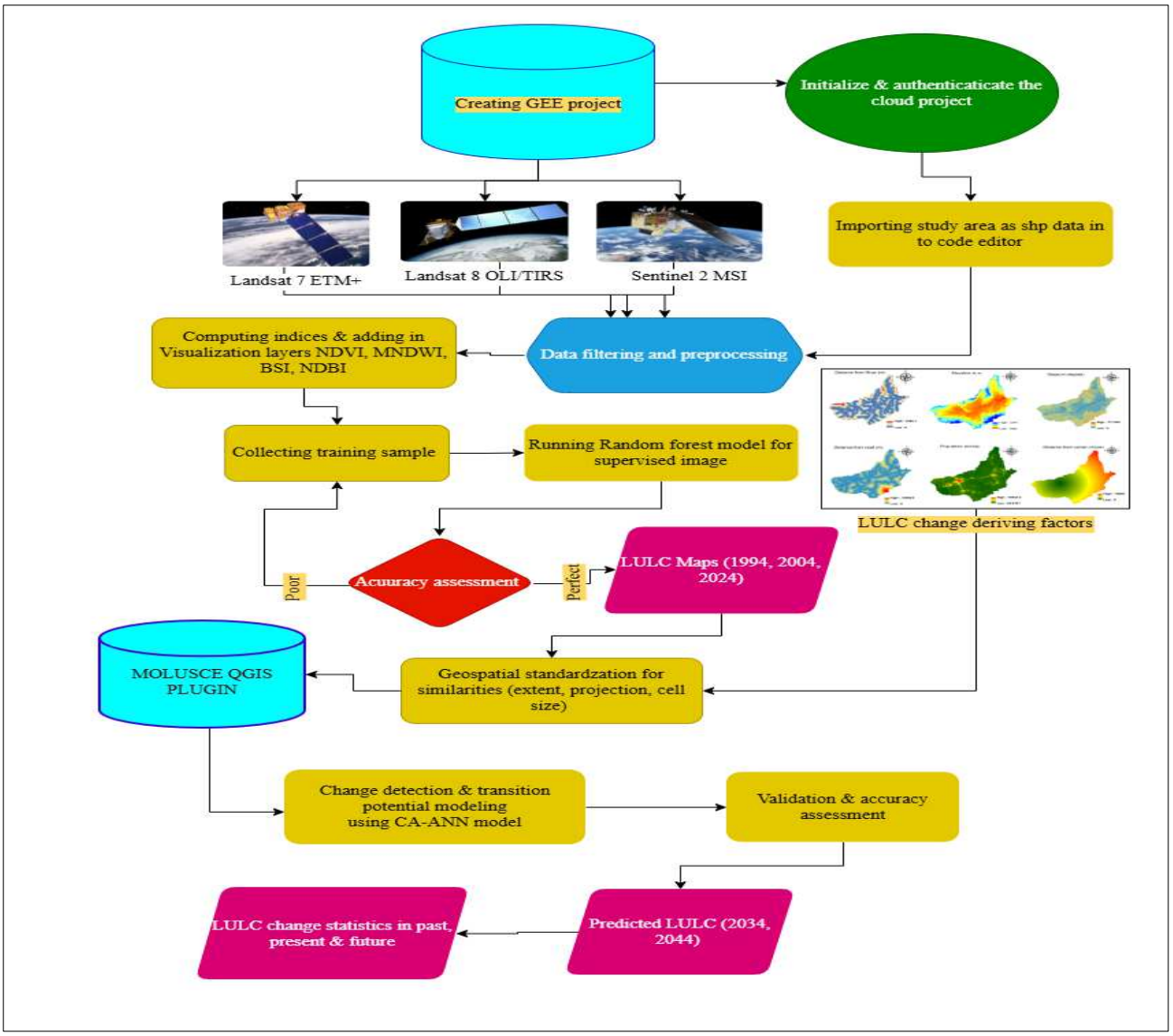


Figure 2 Research methodological flowchart

2.4 Data collection

2.4.1 Satellite Imagery Acquisition

Multi-temporal satellite imagery was acquired from three different sensors through the Google Earth Engine platform to analyze LULC changes across three time periods (Table 1). For the 2004 baseline, Landsat 7 Enhanced Thematic Mapper Plus (ETM+) images at 30 m spatial resolution were obtained from the United States Geological Survey (USGS) covering 2003-2004. The 2014 LULC baseline utilized Landsat 8 Operational Land Imager/Thermal Infrared Sensor (OLI/TIRS) imagery at 30 m resolution acquired between 2013-2014 from USGS via GEE. For model validation and current status assessment, Sentinel-2 Multispectral Instrument (MSI) data at 10 m spatial resolution was collected from the European Space Agency (ESA) through GEE for the 2023-2024 period. Cloud-free Landsat and Sentinel-2 image composites were generated using images acquired during the dry season (November–February) to minimize cloud contamination and seasonal variability. The same seasonal window was maintained across all study years to improve interannual comparability.

Table 1 Multi-temporal satellite imagery specifications

S.N	Sensors	Data source	Spatial resolution	Acquisition year
1	Landsat 7 ETM+	United States Geological Survey (USGS)	30 m	2003- 2004
2	Landsat 8 OLI/TIRS	United States Geological Survey (USGS) via	30 m	2013 - 2014
3	Sentinel-2 MSI	European Space Agency (ESA)	10 m	2023- 2024

2.4.2 Collection of LULC change deriving factors

Six LULC driving factors were identified and their corresponding thematic layers were prepared for the CA-ANN prediction model (Table 2). Elevation data was extracted from ASTER SRTM digital elevation model (DEM) obtained from USGS Earth Explorer. Slope was derived from the DEM using spatial analysis tools in GIS environment. Distance from road was calculated using Euclidean distance analysis on road network data obtained from the Ethiopian Road Authority database. Similarly, distance from town center was computed through Euclidean distance analysis using Ethiopian Urban Master Plan data. Distance from river was determined by first delineating the river network from the DEM through watershed analysis, followed by Euclidean distance computation. Population density data was acquired from the WorldPop dataset and processed through spatial preprocessing techniques.

Table 2 LULC driving factors and data sources

S.N	LULC deriving factors	Raw data source	Data processing method
1	Elevation (EL)	ASTER SRTM USGS https://search.earthdata.nasa.gov/	Direct extraction
2	Slope (SL)	DEM derived	Derived by slope tool spatial analysis
3	Distance from Road (DR)	Ethiopian road authority database	Euclidean distance analysis
4	Distance from center of town	Ethiopian Urban Master Plan data	Euclidean distance analysis
5	Distance from River (DRV)	River network derived from DEM and watershed delineation	Euclidean distance analysis
6	Population density (POD)	WorldPop dataset from https://www.worldpop.org/	Spatial preprocessing

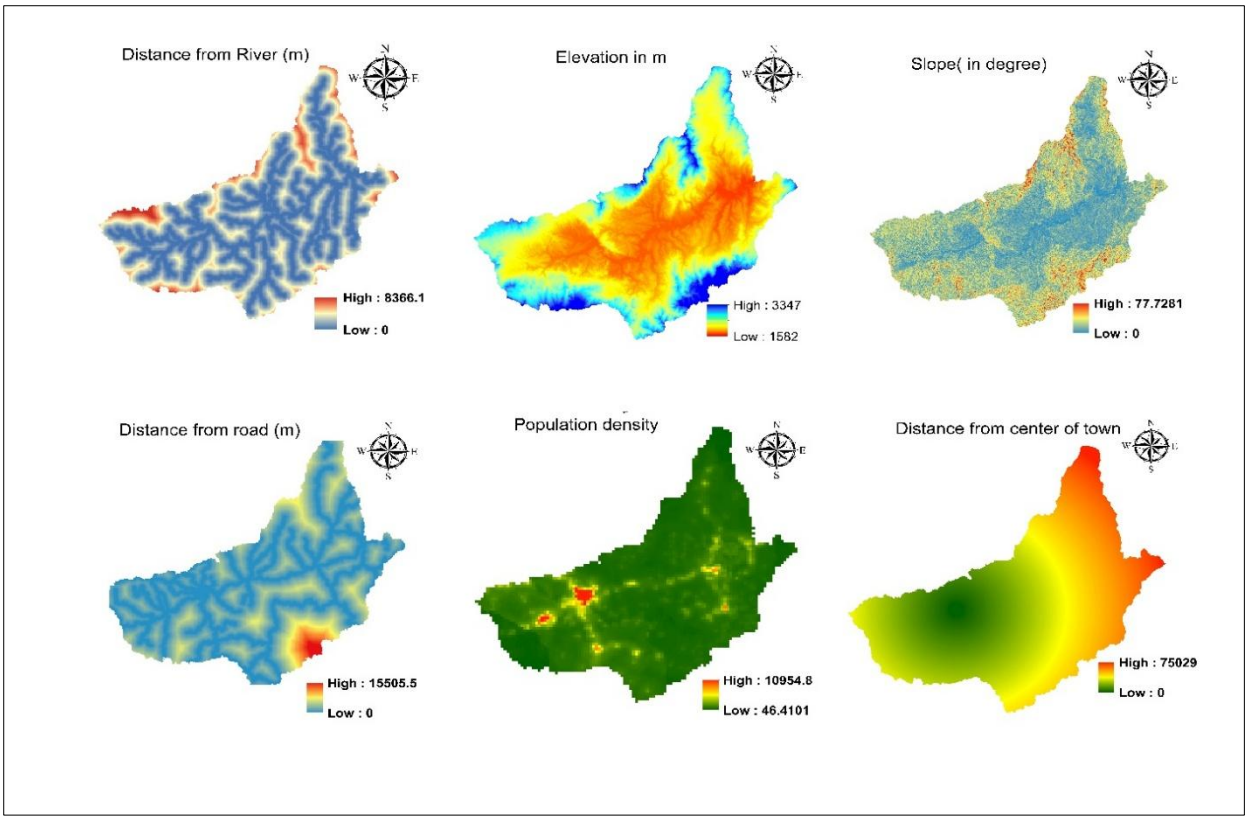


Figure 3 Spatial thematic layers of LULC change deriving factors

2.4.3 Image Preprocessing and Spectral Index Computation

The preprocessing of satellite imagery was conducted using the Google Earth Engine platform, implementing radiometric calibration, atmospheric correction, cloud masking, and temporal compositing. Cloud masking was implemented as a critical preprocessing step to eliminate atmospheric contamination and ensure generation of cloud-free composite images. Radiometric calibration converted digital numbers to surface reflectance values, enabling consistent spectral measurements across different acquisition dates and sensors. Temporal compositing techniques, particularly median composite generation, were employed to create representative imagery for specific time periods while reducing noise and filling data gaps caused by cloud cover.

For Landsat 7 ETM+ imagery affected by the Scan Line Corrector (SLC) failure, multiple observations within the selected temporal window were combined to generate annual composites. The temporal compositing approach substantially reduced data gaps and minimized striping effects associated with SLC-off imagery. Potential scan-line gaps associated with the Landsat 7 SLC-off condition were minimized through the generation of cloud-free multi-date image composites within Google Earth Engine, thereby reducing the influence of missing observations on classification results.

Although the source imagery originated from sensors with different native spatial resolutions, all classified LULC maps were harmonized to a common 30 m spatial resolution prior to change detection analysis and CA-ANN modelling. This harmonization ensured spatial consistency among datasets and reduced potential bias associated with resolution differences between Landsat and Sentinel-2 imagery.

Additionally, spectral indices were computed to enhance discrimination between different LULC classes (Table 3). The Normalized Difference Vegetation Index (NDVI), Normalized Difference Water Index (NDWI), Bare Soil Index (BSI), and Normalized Difference Built-up Index (NDBI) were calculated to improve classification accuracy. The integration of these preprocessing steps within GEE facilitated efficient data handling and significantly reduced processing time compared to traditional desktop-based workflows.

Table 3 Spectral indices computed for LULC classification

Spectral	Formula	Purpose / Application
NDVI	(NIR − Red) / (NIR + Red)	Identify and assess vegetation cover and forested areas
MNDWI	(Green − SWIR) / (Green + SWIR)	Enhanced detection and delineation of surface water bodies
BSI	[(SWIR + Red) − (NIR + Blue)] / [(SWIR + Red) + (NIR + Blue)]	Identify bare land and exposed soil surfaces
NDBI	(SWIR − NIR) / (SWIR + NIR)	Extraction and mapping of built-up and urban areas

2.5 Random Forest Supervised Classification

The land use and land cover classification was performed using the Random Forest (RF) machine learning algorithm implemented in Google Earth Engine (GEE). Random Forest is an ensemble-based classifier that constructs multiple decision trees and determines the final class assignment through majority voting (Kadam et al., 2025). Due to its robustness against overfitting, ability to handle high-dimensional datasets, and strong classification performance in remote sensing applications, RF has become one of the most widely applied algorithms for LULC mapping (Baig et al., 2022; Bîscoveanu et al., 2025; Demessie et al., 2025; Dubertret et al., 2022; Kadam et al., 2025).

Six LULC classes were identified within the watershed: Forest, Water, Built-up, Bare Land, Grassland, and Agriculture. Training samples were collected through stratified random sampling to ensure adequate representation of all classes throughout the watershed. A total of 900 reference samples were collected, comprising approximately 150 samples for each LULC class in 2004, 2014 and 2024 LULC classification. Of these, 840 samples (70%) were used for training and 360 samples (30%) were reserved for validation. Sample collection combined field observations, visual interpretation of high-resolution Google Earth imagery, historical image archives, topographic information, and expert knowledge of local land cover conditions.

To ensure temporal consistency and reduce seasonal variability, satellite images were selected from comparable dry-season periods of the Gilgel Gibe watershed, and the same classification scheme and sampling framework were applied across the 2004, 2014, and 2024 LULC classifications. Landsat imagery for 2004 and 2014 and Sentinel-2 imagery for 2024 were acquired during the dry season (October–April), when cloud cover is minimal and land-cover classes exhibit relatively stable spectral characteristics. Annual median composites were generated from all cloud-free observations within the selected seasonal windows.

For historical classifications (2004 and 2014), training data were generated through visual interpretation of Landsat imagery and historical Google Earth archives, while contemporary classifications (2024) were supported by field observations and recent high-resolution satellite imagery. Ground verification data were collected during field surveys conducted in 2024 using GPS-enabled observations. Ground reference data were collected during

three field survey campaigns conducted in 2024 using GPS-enabled observations. A total of 150 sampling locations were selected to represent the spatial variability of the watershed, encompassing diverse topographic conditions, land-use practices, vegetation types, and environmental settings, thereby ensuring adequate representation of the major LULC classes for classification and validation purposes. Representative samples from all major land cover classes were recorded and subsequently used for training and validation purposes. Multiple geometry sampling approaches, including points, polygons, and line features, were utilized to improve representation of heterogeneous land cover conditions.

Predictor variables used in the classification included all available spectral bands together with derived spectral indices including NDVI, MNDWI, BSI, and NDBI. These variables enhanced the discrimination of vegetation, water bodies, bare surfaces, and built-up features.

The collected reference samples were randomly divided into training (70%) and validation (30%) subsets. The training samples were used to develop the Random Forest classifier, whereas the validation samples were reserved exclusively for independent accuracy assessment and were not used during model training. The validation approach therefore represents a holdout validation design based on independent samples drawn from the overall reference dataset. The classifier was implemented using 500 decision trees, with the square root of the total predictor variables considered at each split. The trained model was subsequently applied to classify Landsat-derived composites for 2004 and 2014 and Sentinel-2 imagery for 2024.

2.6 Accuracy assessment

The accuracy assessment of LULC classification was conducted using confusion matrix analysis, which is a fundamental approach for evaluating the performance of classification algorithms in Google Earth Engine(Bîscoveanu et al., 2025; Deressu et al., 2025). The confusion matrix provides a comprehensive comparison between the classified map and reference data by organizing classification results into a table that displays correct and incorrect classifications for each land cover class (Pan et al., 2022). Classification accuracy was evaluated using a holdout validation approach in which validation samples were randomly separated from the reference dataset prior to model training and subsequently used for independent accuracy assessment.

To evaluate the classification accuracy, multiple statistical metrics were calculated from the confusion matrix. These metrics provide quantitative measures of the classifier's performance and reliability. The primary accuracy metrics employed in this study include Overall Accuracy, Kappa Coefficient, Producer's Accuracy, and User's Accuracy sourced from (Verma et al., 2020).

Overall Accuracy (OA) represents the proportion of correctly classified pixels to the total number of reference pixels and is calculated using the following formula:

$$OA = \frac{\sum_{i=1}^{n} x_{ii}}{N} \times 100 \quad (1)$$

where x_{ii} represents the number of correctly classified pixels in class i (diagonal elements of the confusion matrix), n is the total number of classes, and N is the total number of reference pixels [5]. This metric provides a general measure of classification performance across all land cover classes [6].

Kappa Coefficient (κ) is a robust statistical measure that accounts for the agreement occurring by chance between the classified map and reference data [2]. The Kappa coefficient is calculated as:

$$\kappa = \frac{N \sum_{i=1}^{n} x_{ii} - \sum_{i=1}^{n} (x_{i+} \times x_{+i})}{N^2 - \sum_{i=1}^{n} (x_{i+} \times x_{+i})} \quad (2)$$

where N is the total number of observations, x_{ii} is the number of observations in row i and column i (correctly classified), x_{i+} is the total of row i, and x_{+i} is the total of column i in the confusion matrix [1]. Kappa values range from -1 to 1, where values greater than 0.80 indicate strong agreement, 0.60-0.80 indicate substantial agreement, 0.40-0.60 indicate moderate agreement, and values below 0.40 indicate poor agreement [2].

Producer's Accuracy (PA) measures the probability that a reference pixel is correctly classified and represents the omission error for each class. It is calculated as:

$$PA = \frac{x_{ii}}{x_{+i}} \times 100 \quad (3)$$

where x_{ii} is the number of correctly classified pixels in class i, and x_{+i} is the total number of reference pixels in class i [4].

User's Accuracy (UA) indicates the probability that a pixel classified on the map actually represents that category on the ground and represents the commission error for each class [3]. It is calculated as:

$$UA = \frac{x_{ii}}{x_{i+}} \times 100 \quad (4)$$

where x_{ii} is the number of correctly classified pixels in class i, and x_{i+} is the total number of pixels classified as class i .

The accuracy assessment was implemented in GEE using independent validation samples that were not used during the classifier training phase. This approach ensures an unbiased evaluation of the classification performance and provides reliable accuracy metrics for the LULC map.

2.7 CA-ANN model Implementation and Validation

The Cellular Automata–Artificial Neural Network (CA–ANN) model in MOLUSCE (Modules for Land Use Change Evaluation) plugin in QGIS is used to simulate of future LULC dynamics based on historical transitions and spatial driving forces. The model integrates Markov chain analysis to quantify temporal transition probabilities between LULC classes from classified maps, while the ANN component estimates transition potentials by learning nonlinear relationships between observed LULC changes and multiple explanatory variables, including elevation, slope, distance to roads, distance to rivers, and etc. The CA framework incorporates spatial neighbourhood effects to ensure realistic spatial allocation of predicted land transitions by enforcing contiguity and spatial dependency rules. Model calibration performs using LULC maps from earlier periods, and validation was conducted by comparing the simulated LULC with the observed classification to assess predictive performance. Following satisfactory validation, the calibrated CA–ANN model used to project future LULC scenarios for 2034 and 2044, assuming the persistence of historical transition trends and driving factor influences, thereby enabling spatially explicit prediction of watershed-scale land system dynamics.

Prior to CA–ANN model calibration, the explanatory variables were evaluated using the Pearson correlation coefficient analysis available within the MOLUSCE framework. This procedure was used to identify potential multicollinearity among predictor variables and to support the selection of explanatory factors for model development. The resulting correlation matrix is provided in the Supplementary Material (Figure S5).

By using CA–ANN model, change detection analysis was performed between the 2004 and 2014 LULC maps to identify transition patterns and quantify area changes across different land use classes. Correlation analysis were tested between LULC deriving factors to ensure the relevance for using Pearson correlation method. Then, Transition potential matrices (table) were generated to understand the probability of conversion from one LULC class to another. Transition probabilities were derived from observed land-use changes between historical periods and incorporated into the CA–ANN framework through the transition matrix generated by MOLUSCE. Land-cover transitions were controlled by the transition probability matrix estimated from observed historical changes. Consequently, transitions reflected historically observed landscape dynamics and their associated probabilities. The six spatial driving factors (elevation, slope, distance from road, distance from river, distance from town center, and population density) were integrated as explanatory variables in the CA-ANN model. All explanatory variables were prepared as raster layers with a common coordinate reference system, spatial extent, and cell size to ensure compatibility within the CA–ANN modelling environment. The explanatory variables were treated as static spatial drivers during the simulation period. Consequently, potential future changes in the driving variables themselves were not explicitly modelled. Distance-to-road and distance-to-town-center variables were represented as Euclidean distance rasters generated within the GIS environment and subsequently incorporated into the CA–ANN model as explanatory variables.

The CA–ANN model was calibrated using observed land-use transitions between 2004 and 2014 and subsequently used to simulate the 2024 land-use pattern. The simulated 2024 map was compared with the independently classified 2024 LULC map to evaluate the model's capacity to reproduce observed spatial land-use dynamics. Land-use transition potentials were estimated using the Artificial Neural Network (ANN) module available within the MOLUSCE plugin of QGIS. The ANN implementation is based on a multilayer perceptron structure that learns transition probabilities from historical land-use changes and associated driving variables. The cellular automata component was implemented using the default neighbourhood configuration available within the MOLUSCE framework. The neighbourhood effect was incorporated to account for spatial dependence and local land-use interactions during simulation. Transition potential from year to year was modelling which is input for prediction model and provide deep insight in changes from each class to other. The model simulated LULC for 2024 year were evaluated against classified image in the same year in validation steps. Model in built Kappa statistics report were used to validate the result before going to subsequent prediction for future time at 2034 and 2044. Following successful calibration, the CA-ANN model was executed to predict future LULC scenarios for the years 2034 and 2044. Classification uncertainties and potential temporal inconsistencies among historical and contemporary land-cover datasets may propagate into the CA–ANN validation process and should therefore be considered when interpreting simulation accuracy metrics.

3 Results

3.1 Multi-temporal LULC Classification and Accuracy Assessment

The Random Forest-based supervised classification implemented within Google Earth Engine successfully produced high-resolution LULC maps (figure 4) for the baseline year (2004), mid-period assessment (2014), and contemporary conditions (2024), identifying six distinct land cover classes across the Gibe I Watershed: Forest, Water, Built-up, Bare land, Grassland, and Agriculture. This methodological approach leveraged high-resolution Google Earth imagery combined with extensive ground truth data collected across multiple spatial scales within the watershed, ensuring robust training dataset representation of the diverse landscape characteristics.

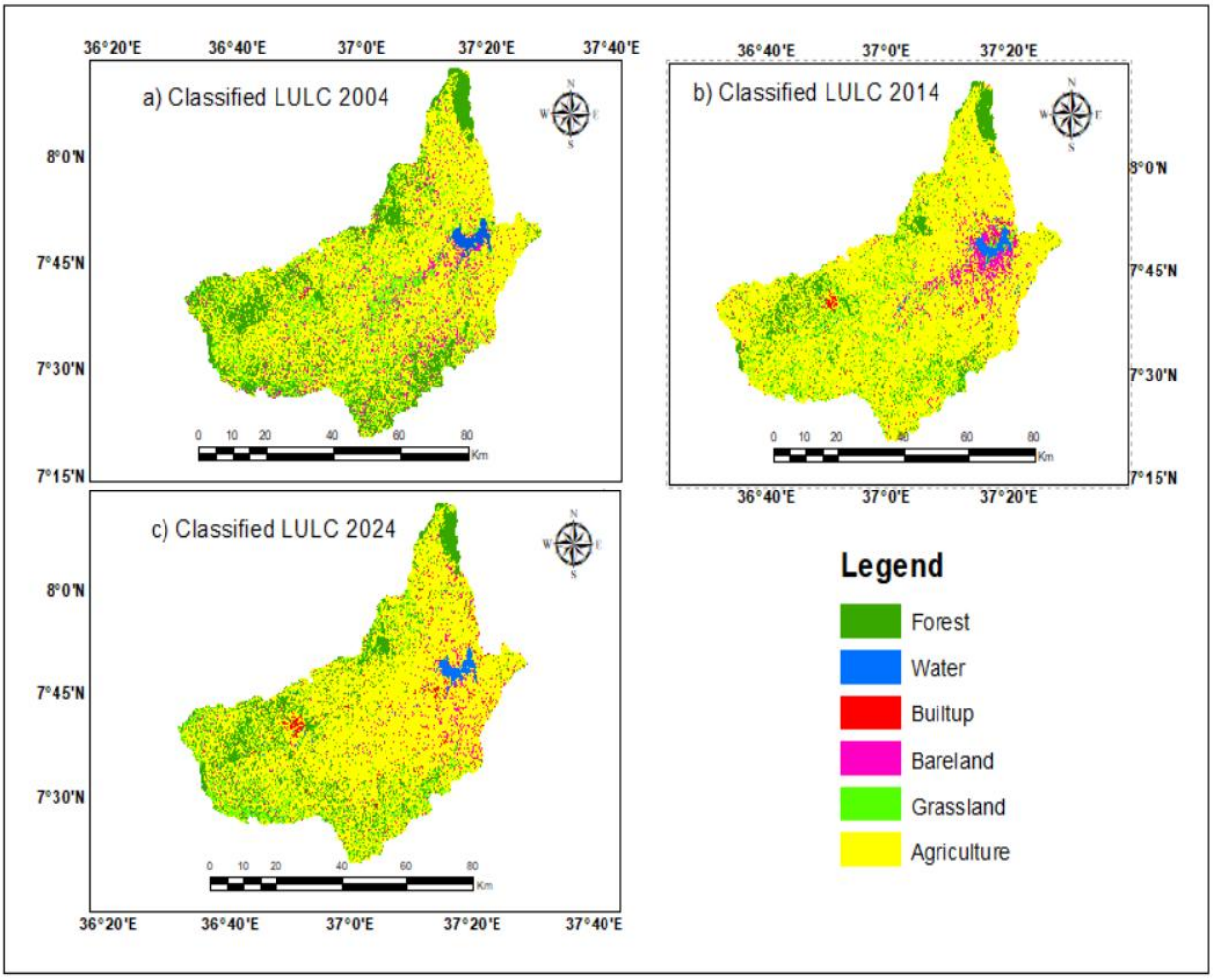


Figure.4. Supervised classification of LULC images for three period a) 2004 b) 2014 c) 2024

Table 4 presents the spatial extent and percentage coverage of each LULC class across the three temporal periods. The classification results reveal pronounced shifts in landscape composition, with Agriculture dominating the watershed area in all periods but showing differential expansion rates.

Table 4 Spatial extent of LULC per classes across 2004, 2014, & 2024

LULC	2004		2014		2024	
types	Area in ha	% Cover	Area in ha	% Cover	Area in ha	% Cover
Forest	85727.05	19.80	42685.00	9.853	35875.52	8.28

Water	5132.72	1.185	5355.11	1.24	5668.65	1.31
Built up	1144.22	0.27	3694.29	0.85	14918.93	3.44
Bare land	27835.86	6.42	19539.74	4.510	12887.35	2.97
Grassland	55375.13	12.78	38472.62	8.88	22825.36	5.27
Agriculture	258001.38	59.55	323469.61	74.67	341221.06	78.77

Accuracy assessment using confusion matrix-derived metrics indicated high classification performance across all periods, with overall accuracies exceeding commonly accepted thresholds for LULC studies (Table 5). The classification performance demonstrated consistent improvement across the temporal sequence, with overall accuracies exceeding 88% for all periods. Specifically, the 2004 baseline classification achieved an overall accuracy of 88.45% with a Kappa coefficient of 0.89, while the 2014 classification improved to 90.62% overall accuracy with a Kappa coefficient of 0.92. The most recent 2024 classification demonstrated the highest performance at 93.8% overall accuracy with a Kappa coefficient of 0.94.

Table 5 Accuracy assessment of LULC classification across three time periods

LULC types	LULC 2004			LULC 2014			LULC 2024		
	UA	PA	F1	UA	PA	F1	UA	PA	F1
Forest	91.64	99.03	95.19	97.26	99.30	98.27	99.64	97.92	98.77
Water	96.08	98.85	97.44	98.97	98.37	98.67	99.99	99.96	99.98
Built-up	78.56	55.36	64.95	87.80	58.78	70.42	99.08	94.86	96.92
Bare land	72.44	90.33	80.40	89.44	97.60	93.34	71.79	47.64	57.28
Grassland	68.72	60.88	64.56	88.11	61.86	72.69	69.12	51.05	58.73
Agriculture	76.68	87.06	81.54	80.21	90.65	85.11	75.80	93.72	83.81
Overall accuracy	88.45%			90.62%			93.8%		
Kappa coefficient	0.89			0.92			0.94		

Detailed confusion matrices for the 2004, 2014, and 2024 classifications are provided in Supplementary Tables S1–S3.

3.2 Historical LULC Change Detection and Transition Dynamics

The Spatio-temporal analysis of LULC change between 2004 and 2024 reveals profound landscape transformation in the Gibe I Watershed, characterized by systematic agricultural expansion coupled with corresponding losses of natural vegetation and forest ecosystems.

Agricultural land represents the dominant and increasingly dominant land system in the watershed. The expansion from 258,001.38 hectares (59.55%) in 2004 to 341,221.06 hectares (78.77%) in 2024 constitutes a net gain of 83,219.68 hectares, equivalent to a 32.2% relative increase. This agricultural expansion demonstrates a differential temporal trajectory: the period from 2004 to 2014 witnessed a rapid 65,468.23 Hectare (25.37% relative) increase, while the subsequent 2014-2024 period showed a more modest 17,752.45 Hectare (5.49% relative) increase.

Forest cover experienced alarming decline, decreasing from 85,727.05 Hectares (19.80%) in 2004 to 35,875.52 hectares (8.28%) in 2024, representing a cumulative loss of 49,851.53 Hectares or 58.15% of the original forest area. This represents a net loss of 43,042.06 hectares in the first decade (2004-2014, representing a 50.21% loss relative to 2004 levels), with continued decline of an additional 6,191.48 hectares in the second decade.

The transition matrix analysis reveals that approximately 85% of forest loss directly converts to agricultural land use, with smaller transitions to grassland and bare land classifications. Notably, regeneration of forest cover is minimal, with only 3,658 hectares of net forest gain documented over the 20-year period, largely confined to areas adjacent to existing forest patches.

Built-up areas exhibited the most dramatic percentage increase among all LULC categories, expanding from 1,144.22 hectares (0.27%) in 2004 to 14,918.93 hectares (3.44%) in 2024, representing a 1,302% relative increase or a net gain of 13,774.71 hectares.

Table 6 LULC change statistics in three seasons

LULC classes	2004-2014		2014 - 2024		2004 - 2024	
	Change in Ha	% Area change	Change in Ha	% Area change	Change in Ha	% Area change
Forest	-43042.06	-50.21	-6,809.48	-1.573	-49,851.53	-58.15
Water	+222.40	+4.33	+313.54	+0.070	+535.93	+10.44
Built up	+2550.07	+222.86	+11,224.64	+303.83	+2550.07	+1,203.82
Bare land	-8296.13	-29.81	-6,652.39	-34.04	-14,948.51	-53.70
Grassland	-16902.50	-30.52	-15,647.26	-40.67	-32,549.77	-58.78
Agriculture	+65468.23	+25.375	+17,751.45	+5.49	+83,219.68	+32.25

Grassland areas experienced substantial decline, decreasing from 55,375 hectares (12.78%) to 22825.36 hectares (5.27%), a loss of 58.78% over the study period. This grassland conversion represents a critical ecological transformation, as these areas traditionally provided essential ecosystem services including carbon sequestration, watershed infiltration, and wildlife habitat. The transition analysis reveals that grassland losses were predominantly converted to agricultural use, with smaller portions transitioning to bare land and built-up areas. The progressive elimination of grasslands threatens pastoral livelihoods dependent upon seasonal pasture availability and reduces ecosystem resilience in semi-arid environments.

Table 7 Loss and gain profile of LULC per classes in 2004 to 2024

LULC classes	Loss in Ha	Gain in Ha	Net change in Ha	% change
Forest	-42365.77	3658.44	-49,851.53	-58.15
Water	-32.45	188.05	+535.93	+10.44
Built up	-114.67	13889.38	+2550.07	+1,203.82
Bare land	-19751.30	6095.34	-14,948.51	-53.70

Grass land	32988.58	8504.6	-32,549.77	-58.78
Agriculture	-17149.05	115368.72	+83,219.68	+32.25

Table 7 presents comprehensive loss and gain profiles for each LULC class, revealing asymmetrical conversion dynamics. Forest class showed 42,365.77 hectares of loss against only 3,658.44 hectares of gain, yielding a net loss of -49,851.53 hectares representing 46.37% of the 2004 baseline. Conversely, Agriculture demonstrated 17,149.05 hectares of loss against 115,368.70 hectares of gain, resulting in 98,219.65 hectares net increase. Built-up areas showed minimal loss (114.67 hectares) against substantial gain (13,889.38 hectares), indicating largely unidirectional expansion. These asymmetrical patterns reflect the irreversible nature of land conversion in the watershed, wherein natural land cover once converted to agriculture remains locked into that use category with minimal reversion to natural states.

3.3 Transition Probability and Land System Conversion Pathways

The transition matrix analysis visualized in Figure 5 elucidates the specific land use conversion pathways driving the aggregate changes. Forest areas showed bidirectional transitions: substantial losses to agriculture (accounting for ~85% of forest loss) and smaller transitions to grassland and bare land. This pattern reveals agriculture as the primary direct deforestation driver. Notably, the analysis indicates limited forest regeneration, with only 3,658 hectares of forest gain documented over the 20-year period, largely confined to areas adjacent to existing forest patches.

Agricultural land transitions reveal complex conversion pathways: while approximately 115,368 hectares of net agricultural gain occurred through primary conversion of forest, grassland, and bare land, analysis shows minor agricultural losses (~17,149 hectares) to built-up expansion and grassland reversion .

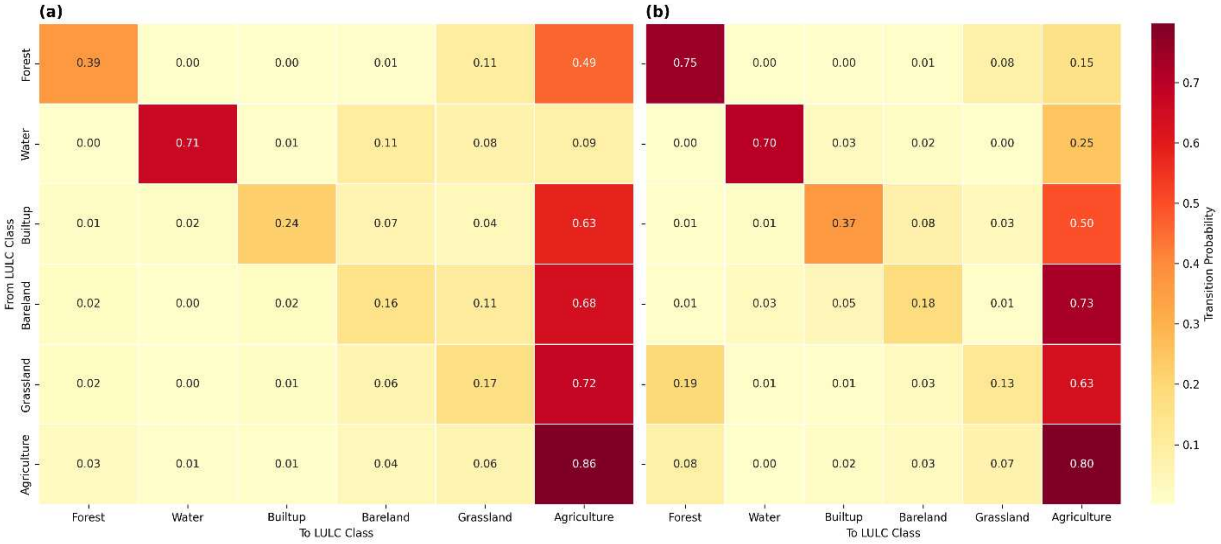


Figure 5 Transition matrix of LULC change between a) 2004 to 2014 b) 2014 to 2024

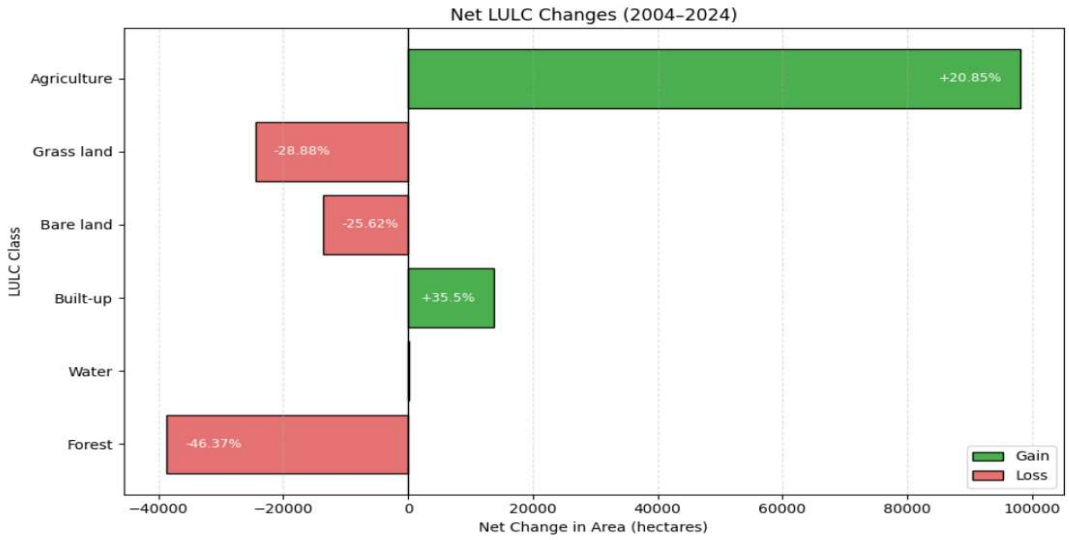


Figure 6. Loss and gain of LULC change in 2004 to 2024

3.4 CA-ANN Model Validation Results

The CA-ANN model demonstrated robust predictive performance when validated against the observed 2024 LULC classification (Table 6). The simulated 2024 LULC map, generated using 2004-2014 baseline data and six driving factors, achieved an overall accuracy of 87.0% with a Kappa coefficient of 0.83 when compared against the actual 2024 Sentinel-2 derived classification. These validation metrics exceed the minimum acceptable thresholds for LULC prediction models and fall within the range of 79-95% overall accuracy reported in the CA-ANN literature globally. The observed agreement indicates that the model was able to reasonably reproduce historical land-use dynamics and provides a useful basis for exploring potential future land-use trajectories under the assumptions of the modelling framework

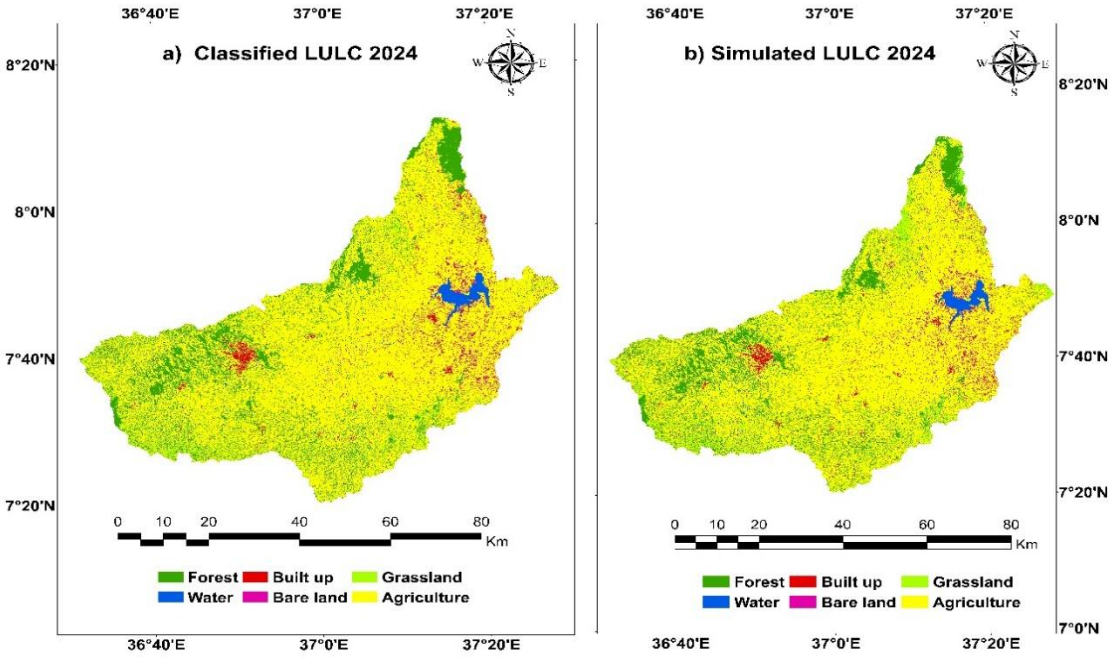


Figure 7 Simulated and classified LULC for 2024 period

Table 8: CA-ANN model validation statistics (Simulated vs. Observed 2024 LULC)

Validation Metric	Value	Interpretation
Overall Accuracy	87.0%	Excellent
Kappa (Overall)	0.83	Strong agreement
Kappa (Location)	0.86	Excellent spatial allocation
Kappa (Histogram)	0.97	Excellent quantitative prediction
Percent Correctness	87.0%	High predictive accuracy

Comparison with other CA-ANN studies in African contexts shows that our model performance is comparable or superior to many published results. For instance, studies in the Upper Omo-Gibe Basin reported overall accuracies of 86.5% (Lukas et al., 2023), while studies in Bangladesh achieved 79.98% accuracy(Uddin, Mahalder, and Mahalder 2023), and studies by Amoah and Gorsevski (2025) in Gana reported accuracies up to 87% [7]. The strong validation results provide confidence in the model's ability to generate reliable future LULC projections for 2034 and 2044. The model built-in validation graph is depicted in fig.8

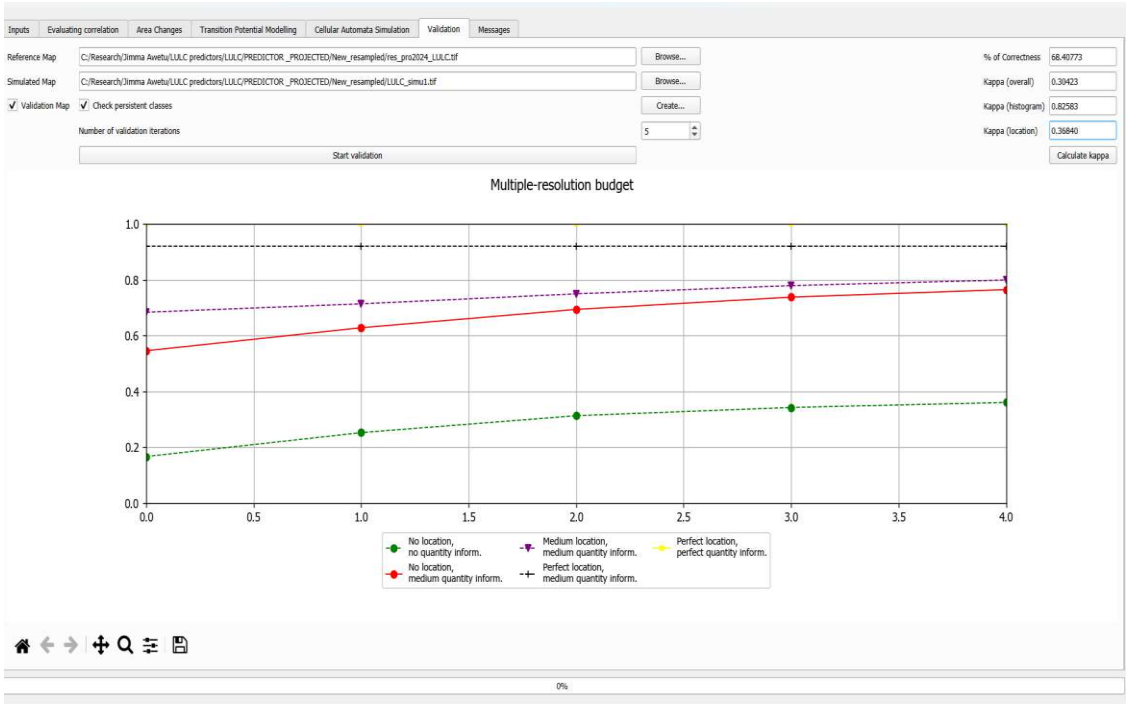


Figure 8 CA-ANN model validation diagram

It should be noted that the observed 2024 LULC map used for validation is itself subject to classification uncertainty. Therefore, agreement statistics obtained during model validation may reflect both model performance and uncertainties associated with the classified reference map.

The model validation result consisting both numerical and graphical in MOLUSCE PLUGIN is depicted in figure 8. The high validation performance reflects the integrated methodology incorporating multiple driving factors through the CA-ANN architecture. The ANN component successfully learned nonlinear relationships between LULC changes observed from 2004-2014 and the explanatory variables. The CA framework enforced spatial contiguity and neighbourhood effects, ensuring realistic spatial allocation consistent with observed land use agglomeration patterns. Notably, Pearson correlation analysis among the six driving factors identified moderate multicollinearity with correlation coefficients typically ranging from 0.35-0.65, suggesting complementary rather than redundant explanatory power.

3.5 Projected LULC Scenarios (2034 and 2044)

The validated CA-ANN model was applied to project future LULC scenarios for 2034 and 2044, assuming continuation of current land transformation trends and persistence of driving factor influences (Table 7). The projections indicate continued expansion of agricultural and built-up areas coupled with progressive decline in forest and grassland cover.

Forest cover decline represents the most critical projected change trajectory. By 2034, forest cover is projected to reach 30,563 hectares (7.06%), and by 2044 to decline further to 28,118 hectares (6.49%), representing cumulative losses of 6,882 hectares and 9,139 hectares respectively from 2024 levels. By 2044, forest cover is projected to decline to a level representing a further 37% reduction from 2024 levels. If these trends continue unabated, the watershed faces the prospect of losing over 75% of its forest cover since 2004, with profound implications for

biodiversity conservation, carbon sequestration, and watershed hydrological functions. This trajectory is particularly concerning given that remaining forest patches are becoming increasingly fragmented and isolated, reducing their capacity to support viable populations of forest-dependent species.

Table 9 Projected LULC and change rate

LULC types	2034 LULC		2044 LULC		% change from 2024 to 2034	% change from 2024 to 2044
	Area in Ha	% cover	Area in Ha	% cover		
Forest	30562.84	7.05 %	28117.82	6.49 %	-14.81	−21.62 %
Water	6044.47	1.39 %	6407.14	1.48 %	+6.63	+13.03 %
Built up	18051.91	4.17 %	24370.08	5.62 %	+21.00	+63.35 %
Bare land	8507.94	1.96 %	5955.56	1.37%	−33.98 %	−53.79 %
Grassland	21623.80	4.99 %	14055.47	3.24 %	−5.26 %	−38.42 %
Agriculture	349096.64	80.55 %	354333.09	81.76 %	+2.31 %	+3.84 %

Agricultural expansion remains the dominant land system trajectory through 2044. Agricultural land is projected to reach 349,097 hectares (80.59%) by 2034 and 354,333 hectares (81.83%) by 2044, representing incremental gains of 13,097 hectares and 18,333 hectares from 2024 levels. This sustained agricultural expansion, reaching 81.3% of the watershed area by 2044, reflects the persistence of population pressure and limited availability of alternative productive land within the region. The projections indicate that agricultural area will stabilize around 81-82% of total watershed area, suggesting a near-complete conversion of arable land at these continuation-of-trends assumptions.

Urbanization and built-up expansion constitute the most rapidly growing land use category by percentage change. Built-up areas are expected to expand from 14,918.93 hectares in 2024 to 18,051.91 hectares by 2034 (a 21% increase) and to escalate to 24,370.08 hectares by 2044 (representing a cumulative 63% increase from 2024 baseline). This accelerating urbanization trajectory aligns with documented national and regional urbanization projections and reflects in-migration associated with rural land degradation and economic opportunities concentrated in urban centers (Amoah and Gorsevski 2025; Sitati et al. 2024; D. Tilahun, Gashu, and Shiferaw 2022; Xu, Zhou, and Li 2022). The doubling of built-up area within the next two decades indicates intensifying land pressures in watershed areas proximal to urban centers and increasing competition for limited land resources between urban expansion and agricultural interests.

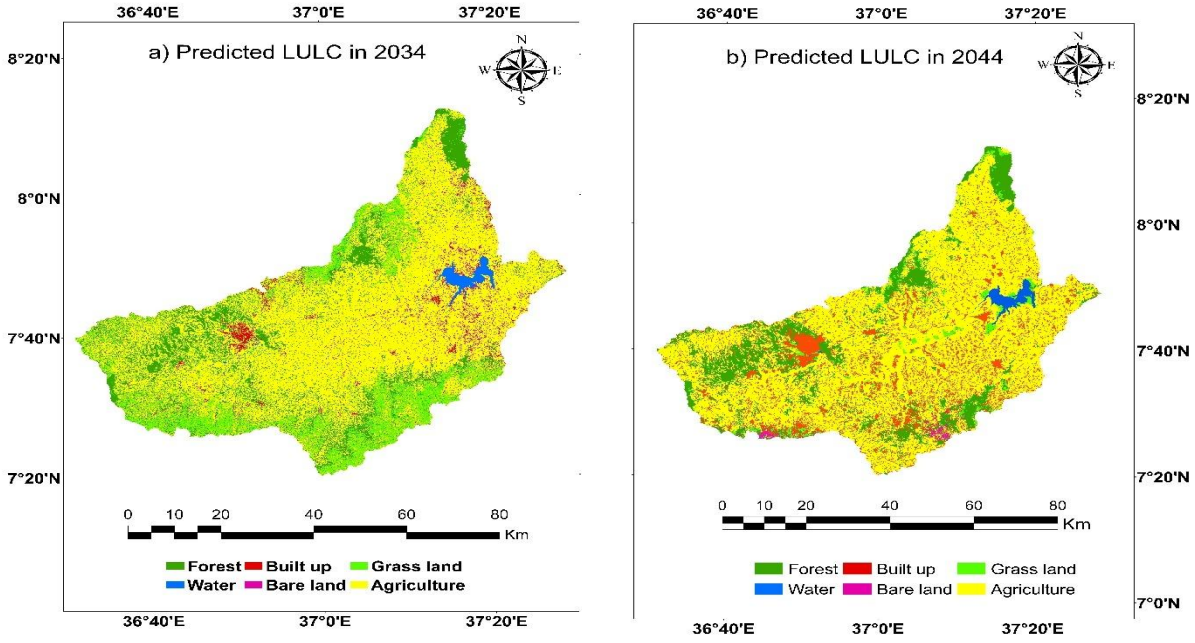


Figure 9 Predicted future LULC for a) 2034 b) 2044

Grassland areas are projected to experience continued decline from 22,825.36 hectares (5.27%) in 2024 to 21,623.80 hectares (4.99%) by 2034 and further to 14,055.47 hectares (3.25%) by 2044, representing cumulative losses of 8,769.89 hectares or 38.4% over the 2024-2044 period. This progressive grassland elimination indicates near-complete conversion of this critical land system in the watershed, with profound implications for pastoral livelihoods and open vegetation ecosystem functions. Bare land is similarly projected to decline from 16,000 hectares (3.69%) in 2024 to 8,507.94 hectares (1.96%) by 2034 and 5,955.16 hectares (1.38%) by 2044, as these areas are converted primarily to agricultural use or stabilized as degraded lands under agricultural management.

Water body coverage shows minimal quantitative change in the projections, with slight increases from baseline 5,668.65 hectares (1.31% in 2024) to 6,407.14 hectares (1.48%) by 2034 and further to 6,044.47 hectares in 2044. These modest increases are attributed to infrastructure development including reservoir construction and water harvesting initiatives. Notably, the small increase in water surface area does not offset the substantial ecosystem services losses associated with forest and grassland conversion. Watershed hydrological function and dry-season baseflow maintenance are fundamentally dependent upon forest cover and grassland infiltration capacity, neither of which are compensated through increased reservoir construction.

Bare land is projected to decline from 12887.35hectares (2.99%) in 2024 to 8,508 hectares (1.96%) by 2034 and 5,956 hectares (1.38%) by 2044, as these areas are converted primarily to agricultural use or remain as degraded lands stabilized under agricultural management. Water bodies show minimal quantitative change in the projections, with slight increases attributed to infrastructure development including reservoir construction and water harvesting initiatives. Notably, the small increase in water surfaces does not offset the ecosystem services losses associated with forest and grassland conversion.

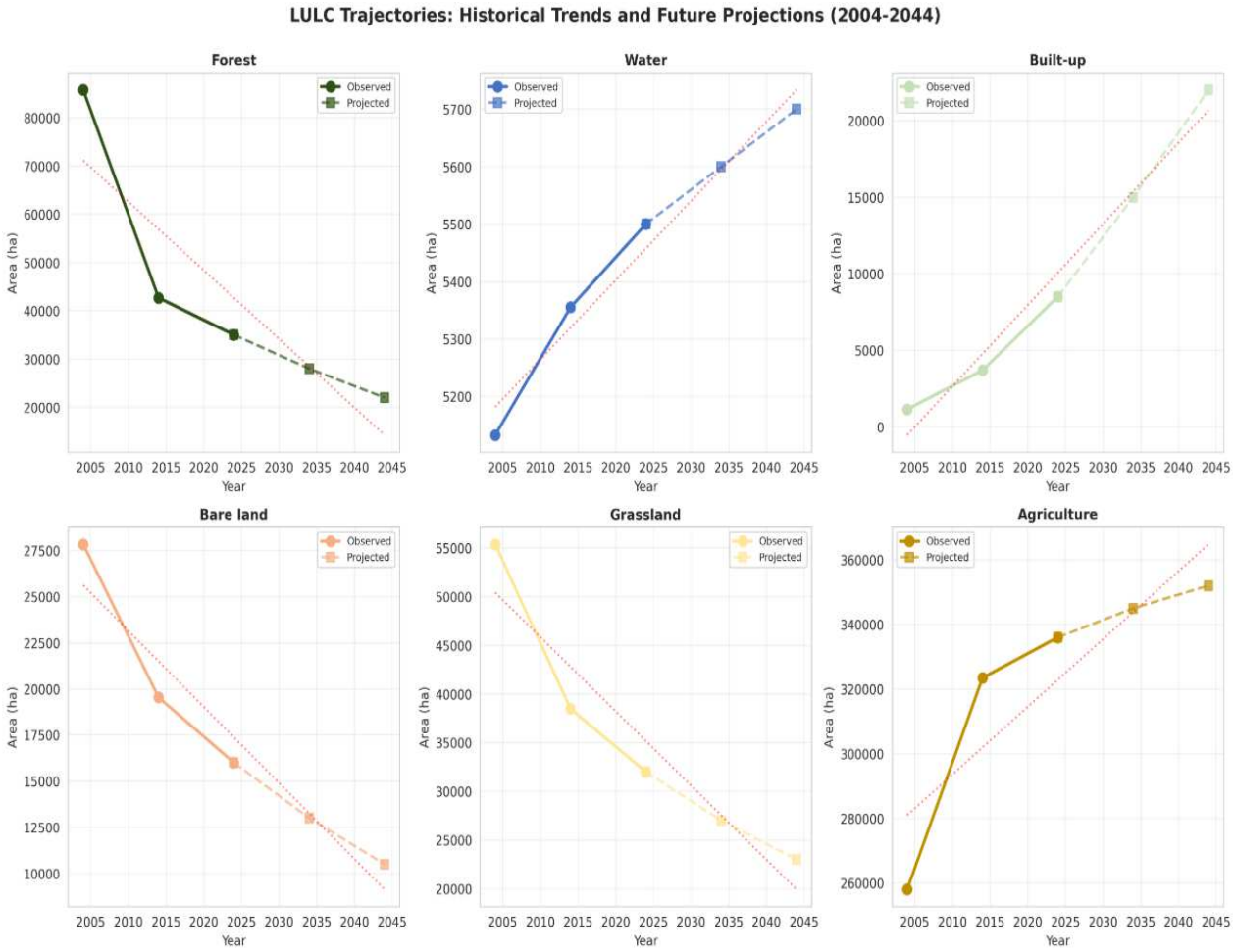


Figure 9 LULC change trajectories

4 Discussion

4.1 Historical LULC dynamics and landscape transformation

The multi-temporal LULC analysis revealed substantial landscape transformation within the Gilgel Gibe I Watershed during the 2004–2024 period. Agriculture remained the dominant land-use class throughout the study period and continued to expand at the expense of forest, grassland, and bare land. Conversely, forest cover exhibited a persistent decline, while built-up areas experienced the highest proportional increase among all land-use classes. These trends indicate increasing anthropogenic pressure on the watershed and reflect the continued conversion of natural land cover into agricultural and settlement areas.

The continued forest decline to 6.49% by 2044 would place the Gibe I Watershed among the most deforested watersheds in the Ethiopian highlands, with critical implications for regional hydrological cycles, carbon stocks, and biodiversity. These projections underscore the urgency of implementing forest conservation and restoration initiatives to alter the current trajectory

The observed LULC dynamics are generally consistent with previous studies conducted in Ethiopia and other tropical watersheds, which similarly reported agricultural expansion and urban growth as dominant patterns of land transformation. Comparable findings by (Derebe et al., 2022; Lukas et al., 2023) have been reported in the Omo-Gibe Basin and other Ethiopian watersheds (Bekele et al., 2025; Edosa & Nagasa, 2024), where population

growth, increasing food demand, and land-use intensification have contributed to widespread conversion of natural vegetation into cultivated land. Likewise, recent studies employing Google Earth Engine and machine-learning classification have documented comparable long-term landscape changes in developing regions (Dubertret et al., 2022; Feng et al., 2022; Fagun et al., 2025).

Although several regional studies associate these trends with demographic growth, agricultural intensification, and land management policies, the present study did not explicitly evaluate socioeconomic or policy drivers. Therefore, these factors should be regarded as plausible explanations supported by previous literature rather than direct findings of this study.

4.2 Land transition patterns and implications for watershed management

The transition matrix analysis demonstrated that forest, grassland, and bare land constituted the principal sources of agricultural expansion. These transition pathways indicate that once natural land cover is converted into agricultural land, relatively little reconversion to natural vegetation occurs, suggesting a largely irreversible pattern of landscape transformation over the study period.

Such transition behaviour has been widely reported in land-change studies across East Africa, where agricultural expansion commonly represents the dominant conversion process affecting watershed ecosystems (Ali et al., 2024; Omer et al., 2023). Continued reduction of natural vegetation may reduce landscape resilience and affect ecological functions such as habitat connectivity and vegetation integrity (Kusiima et al., 2022). However, these potential environmental consequences were not directly quantified in the present study and therefore should be interpreted as literature-based implications rather than direct outcomes of the analysis.

4.3 Performance and applicability of the integrated GEE–RF–CA–ANN framework

The integrated Google Earth Engine, Random Forest, and CA–ANN framework provided reliable historical classification and future LULC simulation for the Gilgel Gibe I Watershed. The high classification accuracies obtained for all three mapping years demonstrate the effectiveness of cloud-based image processing combined with machine-learning classification for regional LULC mapping.

Similarly, the CA–ANN model reproduced the observed 2024 land-use pattern with satisfactory agreement, indicating that the model adequately captured the dominant historical transition processes. Comparable validation accuracies have been reported in previous CA–ANN applications conducted in Ethiopia (Lukas et al., 2023), Ghana (Amoah & Gorsevski, 2025), and Bangladesh (Uddin et al., 2023), demonstrating that the predictive performance obtained in this study exceed the minimum acceptable thresholds for LULC prediction models and fall within the range of 79-95% overall accuracy reported in the CA-ANN literature globally. The observed agreement indicates that the model was able to reasonably reproduce historical land-use dynamics and provides a useful basis for exploring potential future land-use trajectories under the assumptions of the modelling framework

Nevertheless, the reported validation accuracy should not be interpreted as definitive evidence of future prediction certainty. Since the observed 2024 LULC map used for validation is itself subject to classification uncertainty, the model validation inevitably inherits part of these uncertainties. Consequently, the future projections presented in this study should be considered scenario-based estimates derived from historical transition patterns rather than deterministic forecasts.

4.4 Future land-use scenarios and planning implications

The projected scenarios for 2034 and 2044 suggest continued expansion of agricultural and built-up land, accompanied by further reductions in forest and grassland cover if current land-use trends continue. These projected changes highlight the potential for increasing pressure on remaining natural ecosystems within the watershed. The Gibe I Watershed projections align with these regional patterns, indicating that current land conversion drivers are likely to persist without substantial policy intervention. The projected 81.3% agricultural coverage by 2044 approaches saturation of agricultural land availability, suggesting that near-term future changes may be constrained by limited remaining natural land cover available for conversion.

Rather than representing certain future outcomes, these projections should be interpreted as plausible scenarios based on historical transition probabilities and the selected spatial driving factors. They therefore provide useful spatial information for watershed planning, land resource management, and environmental decision-making by identifying areas that may experience continued land transformation under current development trajectories.

The projected changes also emphasize the importance of balancing agricultural development with sustainable land management strategies that support ecosystem conservation and long-term watershed resilience.

4.5 Eco-hydrological implication of the LULC change

The projected landscape transformations through 2044 carry profound implications for watershed ecosystem services, hydrological function, and long-term environmental sustainability. These implications extend beyond the watershed boundaries to affect downstream water resources and hydropower generation sustainability.

The projected loss of an additional 7,757.70 hectares of forest by 2044 (cumulative loss of 57,609.23 hectares from 2004 levels) fundamentally alters watershed hydrological processes. Forest loss in the Omo-Gibe Basin has been directly linked to increased soil erosion rates, with research documenting erosion increases of 25-40% following deforestation (A. B. Aneseyee et al., 2020; E. T. Mekuria et al., 2025; Toma et al., 2023). The conversion of forest to agricultural land drastically reduces watershed infiltration capacity and increases surface runoff generation, mechanisms that potentially exacerbate flooding risks during high-intensity precipitation events while simultaneously reducing dry-season baseflow essential for sustaining human and ecological water demands. Ecosystem service valuation studies in Ethiopian highlands have quantified forest loss costs at $40-60 million annually due to reduced water regulation, soil retention, and carbon sequestration services (Mathewos & Aga, 2023; W. Mekuria et al., 2021). The Gibe I Watershed losses represent a substantial contribution to these regional ecosystem service deficits.

The expansion of agricultural land to 81% of the watershed by 2044 raises critical concerns regarding long-term sustainability and land degradation trajectory. Intensive cultivation on steep slopes without adequate soil conservation measures accelerates land degradation processes, reducing soil productivity and increasing erosion susceptibility. Studies in the broader Omo-Gibe Basin have documented sediment yield increases of 18-28% associated with agricultural expansion (A. B. Aneseyee et al., 2020; Estifanos & Gebremariam, 2020; Toma et al., 2023), directly threatening reservoir capacity maintenance and hydropower generation sustainability. The Gibe I Watershed, as a component of the broader Omo-Gibe system, supplies water to multiple hydropower facilities critical for national electricity generation (Fanta et al., 2022; Z. A. Tilahun et al., 2023). Accelerated

sedimentation reduces reservoir lifespan and hydropower productivity, creating downstream implications extending beyond the immediate watershed.

The projected dramatic decline in grasslands, from 5.27% to 3.25% of watershed area by 2044, threatens pastoral livelihoods and food security. Grasslands serve critical roles in livestock production and dry-season fodder supply essential for pastoral communities. The loss of 8,769.89 hectares of grassland over two decades eliminates critical grazing resources and reduces ecosystem resilience to drought events increasingly frequent under climate change scenarios. The synergistic effects of grassland loss create compounding vulnerabilities for pastoral populations dependent upon these ecosystem services.

These findings underscore the urgent need for integrated watershed management strategies that balance development needs with environmental sustainability. Priority interventions should include: (1) strengthening enforcement of existing forest protection policies and expanding protected area networks in remaining high-biodiversity zones ; (2) promoting sustainable agricultural intensification on existing croplands rather than extensification into forests ; (3) implementing payment for ecosystem services schemes to provide economic incentives for forest conservation; and (4) integrating LULC projections into spatial planning frameworks to proactively manage urbanization and infrastructure development. The Green Legacy Initiative should be scaled up with particular focus on reforestation of degraded lands and agroforestry systems that integrate conservation with livelihood objectives.

4.6 Study limitations and future research

Several limitations should be considered when interpreting the results of this study. First, although historical and contemporary satellite datasets were harmonized before change analysis, differences in sensor characteristics may still introduce minor uncertainties in LULC classification. Second, the CA–ANN model assumes that historical land transition behaviour and explanatory variables remain representative of future conditions, whereas socioeconomic development, infrastructure expansion, and policy interventions may alter future land-use trajectories.

In addition, the explanatory variables were treated as static spatial drivers throughout the simulation period, and uncertainty analysis, sensitivity analysis, and alternative scenario modelling were beyond the scope of the present study. Furthermore, the environmental implications discussed, including potential effects on runoff, soil erosion, sediment transport, and ecosystem services, were inferred from previous studies and were not directly quantified.

Future studies could improve prediction reliability by incorporating dynamic socioeconomic datasets, climate projections, policy scenarios, and explainable artificial intelligence techniques for improved interpretation of model behaviour. Integrating hydrological and ecosystem-service models with future LULC simulations would also provide a more comprehensive understanding of the environmental consequences of landscape change.

5 Conclusions

This study successfully integrated Google Earth Engine cloud-based remote sensing, Random Forest machine learning classification, and CA-ANN prediction modelling to comprehensively assess LULC dynamics in the Gibe I Watershed, Ethiopia. The Random Forest classification identified six land cover types in the watershed and

achieved excellent accuracies consistently exceeding Overall accuracy of 85%, demonstrating the effectiveness of GEE-based approaches for LULC monitoring in tropical and subtropical watersheds. Historical analysis spanning 2004-2024 revealed dramatic landscape transformations, with agricultural land and built up expanding by 32.2% and 1203.6% respectively, while forest cover declined by 58.15%, driven by population pressure, agricultural intensification, and urbanization pressures. The validated CA-ANN model (87% accuracy, Kappa 0.83) projects continued expansion of agricultural and built-up areas through 2044, with forest cover potentially declining to 6.49% of the watershed, approaching critical thresholds for ecosystem service provision and biodiversity conservation.

These findings provide critical evidence-based insights for sustainable land management and conservation planning in the Omo-Gibe Basin and demonstrate the applicability of integrated remote sensing and predictive modelling approaches for evidence-based watershed management. The integration of cutting-edge remote sensing technologies with validated prediction models offers a replicable methodological framework for LULC monitoring in data-scarce regions globally. The future land-use simulations presented in this study represent projections based on historical transition patterns and the selected driving factors. Uncertainty analysis, sensitivity testing, and alternative scenario development were beyond the scope of the current work but constitute important directions for future research to further evaluate model robustness and projection uncertainty.

Future research should incorporate high-resolution imagery, additional socio-economic driving factors, alternative scenario development incorporating policy intervention strategies, and explicit modelling of ecosystem service impacts to further enhance decision-support capabilities for watershed management authorities and policymakers.

References

Aldiansyah, S., & Saputra, R. A. (2022). COMPARISON OF MACHINE LEARNING ALGORITHMS FOR LAND USE AND LAND COVER ANALYSIS USING GOOGLE EARTH ENGINE (CASE STUDY: WANGGU WATERSHED). *International Journal of Remote Sensing and Earth Sciences*, *19*(2), 197–210. https://doi.org/10.30536/ijreses.v19i2.13716

Ali, M., Ali, T., Gawai, R., Dronjak, L., & Elaksher, A. (2024). The Analysis of Land Use and Climate Change Impacts on Lake Victoria Basin Using Multi-Source Remote Sensing Data and Google Earth Engine (GEE). *Remote Sensing*, *16*(24), 4810. https://doi.org/10.3390/rs16244810

Alshehri, B., Zhang, Z., & Liu, X. (2025). A Review of Google Earth Engine for Land Use and Land Cover Change Analysis: Trends, Applications, and Challenges. *ISPRS International Journal of Geo-Information*, *14*(11). https://doi.org/10.3390/ijgi14110416

Amoah, M. K. M., & Gorsevski, P. V. (2025). Predicting land use land cover changes and impact on urban wetlands using cellular automata and artificial neural networks approach, a case study in Greater Accra, Ghana. *Scientific African*, *28*, e02767. https://doi.org/10.1016/j.sciaf.2025.e02767

Aneseyee, A. B., Elias, E., Soromessa, T., & Feyisa, G. L. (2020). Land use/land cover change effect on soil erosion and sediment delivery in the Winike watershed, Omo Gibe Basin, Ethiopia. *Science of The Total Environment*, *728*, 138776. https://doi.org/10.1016/j.scitotenv.2020.138776

Aneseyee, A., Soromessa, T., & Elias, E. (2019). The effect of land use/land cover changes on ecosystem services valuation of Winike watershed, Omo Gibe basin, Ethiopia. *Human and Ecological Risk Assessment: An International Journal*, *26*, 1–20. https://doi.org/10.1080/10807039.2019.1675139

Baidoo, R., Arko-Adjei, A., Poku-Boansi, M., Quaye-Ballard, J. A., & Somuah, D. P. (2023). Land use and land cover changes implications on biodiversity in the Owabi catchment of Atwima Nwabiagya North District, Ghana. *Heliyon*, *9*(5), e15238. https://doi.org/10.1016/j.heliyon.2023.e15238

Baig, M. F., Mustafa, M. R. U., Baig, I., Takaijudin, H. B., & Zeshan, M. T. (2022). Assessment of Land Use Land Cover Changes and Future Predictions Using CA-ANN Simulation for Selangor, Malaysia. *Water*, *14*(3). https://doi.org/10.3390/w14030402

Bekele, T., Kebede, A., & Moges, A. (2025). Land Use and Land Cover Dynamics in the Bilate Subbasin, Southern Ethiopia: Analyzing Key Processes and Driving Factors. *Advances in Agriculture*, *2025*(1), 2493364. https://doi.org/10.1155/aia/2493364

Bîscoveanu, O. M., Badea, G., Dragomir, P. I., & Badea, A. C. (2025). Evaluation of LULC Use Classification for the Municipality of Deva, Hunedoara County, Romania Using Sentinel 2A Multispectral Satellite Imagery—A Comparative Study of GIS Software Analysis and Accuracy Assessment. *Applied Sciences*, *15*(21). https://doi.org/10.3390/app152111437

Blissag, B., Yebdri, D., & Kessar, C. (2024). Spatiotemporal change analysis of LULC using remote sensing and CA-ANN approach in the Hodna basin, NE of Algeria. *Physics and Chemistry of the Earth, Parts A/B/C*, *133*, 103535. https://doi.org/10.1016/j.pce.2023.103535

Bosma, C., & Hein, L. (2023). The climate and land use change nexus: Implications for designing adaptation and conservation investment strategies in Sub-Saharan Africa. *Sustainable Development*, *31*(5), 3811–3830. https://doi.org/10.1002/sd.2627

Brunori, E., Salvati, L., Mancinelli, R., Smiraglia, D., & Biasi, R. (2017). Multi-temporal land use and cover changing analysis: The environmental impact in Mediterranean area. *International Journal of Sustainable Development & World Ecology*, *24*(3), 276–288. https://doi.org/10.1080/13504509.2016.1205156

Dagnachew, M., Kebede, A., Moges, A., & Abebe, A. (2020). Land Use Land Cover Changes and Its drivers in Gojeb River Catchment, Omo Gibe Basin, Ethiopia. *Journal of Agriculture and Environment for International Development (JAEID)*, *114*(1), 33–56. https://doi.org/10.12895/jaeid.20201.842

Değermenci, A. S. (2023). Spatio-temporal change analysis and prediction of land use and land cover changes using CA-ANN model. *Environmental Monitoring and Assessment*, *195*(10), 1229. https://doi.org/10.1007/s10661-023-11848-9

Demessie, S. F., Dile, Y. T., Bedadi, B., Tarkegn, T. G., Bayabil, H. K., & Sintayehu, D. W. (2025). Assessing and projecting land use land cover changes using machine learning models in the Guder watershed, Ethiopia. *Environmental Challenges*, *18*, 101074. https://doi.org/10.1016/j.envc.2024.101074

Derebe, M. A., Hatiye, S. D., & Asres, L. A. (2022). Dynamics and Prediction of Land Use and Land Cover Changes Using Geospatial Techniques in Abelti Watershed, Omo Gibe River Basin, Ethiopia. *Advances in Agriculture*, *2022*(1), 1862461. https://doi.org/10.1155/2022/1862461

Deressu, T. F., Bojer, A. K., Debelee, T. G., Negera, W. G., Nadarajah, S., & Gebissa, K. W. (2025). Enhancing land use and land cover classification with deep learning-based satellite imagery segmentation. *International Journal of Applied Earth Observation and Geoinformation*, *144*, 104839. https://doi.org/10.1016/j.jag.2025.104839

Dubertret, F., Tourneau, F.-M. L., Villarreal, M. L., & Norman, L. M. (2022). Monitoring Annual Land Use/Land Cover Change in the Tucson Metropolitan Area with Google Earth Engine (1986–2020). *Remote Sensing*, *14*(9). https://doi.org/10.3390/rs14092127

Edosa, B. T., & Nagasa, M. D. (2024). Spatiotemporal assessment of land use land cover change, driving forces, and consequences using geospatial techniques: The case of Naqamte city and hinterland, western Ethiopia. *Environmental Challenges*, *14*, 100830. https://doi.org/10.1016/j.envc.2023.100830

Estifanos, T. H., & Gebremariam, B. (2020). Modeling-impact of Land Use/Cover Change on Sediment Yield (Case Study on Omo-gibe Basin, Gilgel Gibe III Watershed, Ethiopia). *American Journal of Modern Energy*, *5*(6), 84–93. https://doi.org/10.11648/j.ajme.20190506.11

Fagun, I. A., Islam, Md. R., Shipra, N. T., Kunda, M., Harun-Al-Rashid, A., & Afandi, G. E. (2025). Spatiotemporal Analysis of LULC in a Wetland Ecosystem of Bangladesh Using Google Earth Engine and Machine Learning Approach. *Earth Systems and Environment*. https://doi.org/10.1007/s41748-025-00909-3

Fanta, S. S., Namara, W. G., & Yesuf, M. B. (2022). Assessment of water supply and demand in Gilgel Gibe watershed, southwest Ethiopia. *Sustainable Water Resources Management*, *8*(4), 104. https://doi.org/10.1007/s40899-022-00684-3

Feng, S., Li, W., Xu, J., Liang, T., Ma, X., Wang, W., & Yu, H. (2022). Land Use/Land Cover Mapping Based on GEE for the Monitoring of Changes in Ecosystem Types in the Upper Yellow River Basin over the Tibetan Plateau. *Remote Sensing*, *14*(21). https://doi.org/10.3390/rs14215361

Fontana, A. G., Nascimento, V. F., Ometto, J. P., & do Amaral, F. H. F. (2023). Analysis of past and future urban growth on a regional scale using remote sensing and machine learning. *Frontiers in Remote Sensing*, *4*. https://doi.org/10.3389/frsen.2023.1123254

Gorelick, N., Hancher, M., Dixon, M., Ilyushchenko, S., Thau, D., & Moore, R. (2017). Google Earth Engine: Planetary-scale geospatial analysis for everyone. *Remote Sensing of Environment, Big Remotely Sensed Data: Tools, Applications and Experiences*, *202*, 18–27. https://doi.org/10.1016/j.rse.2017.06.031

Hosseini, H., Atazadeh, B., & Rajabifard, A. (2025). Towards intelligent land administration systems: Research challenges, applications and prospects in AI-driven approaches. *Land Use Policy*, *157*, 107652. https://doi.org/10.1016/j.landusepol.2025.107652

Islam, Md. Y., Nasher, N. M. R., Karim, K. H. R., & Rashid, K. J. (2023). Quantifying forest land-use changes using remote-sensing and CA-ANN model of Madhupur Sal Forests, Bangladesh. *Heliyon*, *9*(5), e15617. https://doi.org/10.1016/j.heliyon.2023.e15617

Jamei, Y., Seyedmahmoudian, M., Jamei, E., Horan, B., Mekhilef, S., & Stojcevski, A. (2022). Investigating the Relationship between Land Use/Land Cover Change and Land Surface Temperature Using Google Earth Engine; Case Study: Melbourne, Australia. *Sustainability*, *14*(22). https://doi.org/10.3390/su142214868

Kadam, S., Kadam, A., Jamdade, S., Rathi, N., Gadilkar, A., ohri, C., Gujar, J., & Kale, R. (2025). Evaluation of Random Forest algorithms for mapping of land use land cover using remote sensing data for Baitarani River. *International Journal of Information Technology*, *17*(6), 3639–3648. https://doi.org/10.1007/s41870-025-02411-5

Kariuki, R. W., Munishi, L. K., Courtney-Mustaphi, C. J., Capitani, C., Shoemaker, A., Lane, P. J., & Marchant, R. (2021). Integrating stakeholders' perspectives and spatial modelling to develop scenarios of future land use and land cover change in northern Tanzania. *PLOS ONE*, *16*(2), e0245516. https://doi.org/10.1371/journal.pone.0245516

Khan, M., & Chen, R. (2025). Assessing the Impact of Land Use and Land Cover Change on Environmental Parameters in Khyber Pakhtunkhwa, Pakistan: A Comprehensive Study and Future Projections. *Remote Sensing*, *17*(1). https://doi.org/10.3390/rs17010170

Kumar, L., & Mutanga, O. (2018). Google Earth Engine Applications Since Inception: Usage, Trends, and Potential. *Remote Sensing*, *10*(10). https://doi.org/10.3390/rs10101509

Kusiima, S. K., Egeru, A., Namaalwa, J., Byakagaba, P., Mfitumukiza, D., Mukwaya, P., Mensah, S., & Asiimwe, R. (2022). Interconnectedness of Ecosystem Services Potential with Land Use/Land Cover Change Dynamics in Western Uganda. *Land*, *11*(11). https://doi.org/10.3390/land11112056

Lukas, P., Melesse, A. M., & Kenea, T. T. (2023). Prediction of Future Land Use/Land Cover Changes Using a Coupled CA-ANN Model in the Upper Omo–Gibe River Basin, Ethiopia. *Remote Sensing*, *15*(4). https://doi.org/10.3390/rs15041148

Mafiana, C. F., Izunobi, J. U., Iduseri, E. O., Abbas, I. I., & Kama, H. G. (2025). Sustainable development goals and effects of Land-Use–Land-Cover (LULC) changes on vegetation using Kubanni River Basin, Zaria, Nigeria as a case-in-point. *Ecohydrology & Hydrobiology*, *25*(4), 100694. https://doi.org/10.1016/j.ecohyd.2025.100694

Makwinja, R., Kaunda, E., Mengistou, S., & Alamirew, T. (2021). Impact of land use/land cover dynamics on ecosystem service value—A case from Lake Malombe, Southern Malawi. *Environmental Monitoring and Assessment*, *193*(8), 492. https://doi.org/10.1007/s10661-021-09241-5

Mathewos, M., & Aga, A. O. (2023). Evaluation of the Linkages between Ecosystem Services and Land Use/Land Cover Changes in Matenchose Watershed, Rift Valley Basin, Ethiopia. *Quaternary*, *6*(1). https://doi.org/10.3390/quat6010013

Mekuria, E. T., Demissie, T. A., & Feyessa, F. F. (2025). Investigation of the spatial and temporal long-term hydro-climatic trends in Upper Omo Gibe Basin, Ethiopia. *Heliyon*, *11*(3), e42265. https://doi.org/10.1016/j.heliyon.2025.e42265

Mekuria, W., Diyasa, M., Tengberg, A., & Haileslassie, A. (2021). Effects of Long-Term Land Use and Land Cover Changes on Ecosystem Service Values: An Example from the Central Rift Valley, Ethiopia. *Land*, *10*(12). https://doi.org/10.3390/land10121373

Midekisa, A., Holl, F., Savory, D. J., Andrade-Pacheco, R., Gething, P. W., Bennett, A., & Sturrock, H. J. W. (2017). Mapping land cover change over continental Africa using Landsat and Google Earth Engine cloud computing. *PLOS ONE*, *12*(9), e0184926. https://doi.org/10.1371/journal.pone.0184926

Muhammad, R., Zhang, W., Abbas, Z., Guo, F., & Gwiazdzinski, L. (2022). Spatiotemporal Change Analysis and Prediction of Future Land Use and Land Cover Changes Using QGIS MOLUSCE Plugin and Remote Sensing Big Data: A Case Study of Linyi, China. *Land*, *11*(3). https://doi.org/10.3390/land11030419

Omer, A., Yuan, X., & Gemitzi, A. (2023). Transboundary Nile basin dynamics: Land use change, drivers, and hydrological impacts under socioeconomic pathways. *Ecological Indicators*, *153*, 110414. https://doi.org/10.1016/j.ecolind.2023.110414

Orkodjo, T. P., Kranjac-Berisavijevic, G., & Abagale, F. K. (2022). Impact of climate change on future availability of water for irrigation and hydropower generation in the Omo-Gibe Basin of Ethiopia. *Journal of Hydrology: Regional Studies*, *44*, 101254. https://doi.org/10.1016/j.ejrh.2022.101254

Pan, X., Wang, Z., Gao, Y., Dang, X., & Han, Y. (2022). Detailed and automated classification of land use/land cover using machine learning algorithms in Google Earth Engine. *Geocarto International*, *37*(18), 5415–5432. https://doi.org/10.1080/10106049.2021.1917005

Pereira, C. O., Escanilla-Minchel, R., González, A. C., Alcayaga, H., Aguayo, M., Arias, M. A., & Flores, A. N. (2022). Assessment of Future Land Use/Land Cover Scenarios on the Hydrology of a Coastal Basin in South-Central Chile. *Sustainability*, *14*(24), 16363. https://doi.org/10.3390/su142416363

Raguraman, N., & Bhardwaj, A. (2024). Spatial Analysis of Land Use Land Cover Dynamics in the Madurai District Using Sentinel-2 Data and Supervised Learning Algorithms. *The International Archives of the Photogrammetry, Remote Sensing and Spatial Information Sciences*, *XLVIII-4–2024*, 367–372. ISPRS TC IV Mid-term Symposium “Spatial Information to Empower the Metaverse” - 22–25 October 2024, Fremantle, Perth, Australia. https://doi.org/10.5194/isprs-archives-XLVIII-4-2024-367-2024

Shimizu, K., Murakami, W., Furuichi, T., & Estoque, R. C. (2023). Mapping Land Use/Land Cover Changes and Forest Disturbances in Vietnam Using a Landsat Temporal Segmentation Algorithm. *Remote Sensing*, *15*(3). https://doi.org/10.3390/rs15030851

Sitati, E. N., Abdallah, S., Olago, D., & Marchant, R. (2024). Past and Future Land Use and Land Cover Trends across the Mara Landscape and the Wider Mau River Basin, Kenya. *Land*, *13*(9). https://doi.org/10.3390/land13091443

Talukdar, S., Singha, P., Mahato, S., Shahfahad, Pal, S., Liou, Y.-A., & Rahman, A. (2020). Land-Use Land-Cover Classification by Machine Learning Classifiers for Satellite Observations—A Review. *Remote Sensing*, *12*(7). https://doi.org/10.3390/rs12071135

Tamiminia, H., Salehi, B., Mahdianpari, M., Quackenbush, L., Adeli, S., & Brisco, B. (2020). Google Earth Engine for geo-big data applications: A meta-analysis and systematic review. *ISPRS Journal of Photogrammetry and Remote Sensing*, *164*, 152–170. https://doi.org/10.1016/j.isprsjprs.2020.04.001

Thakur, P. K., Thakur, P. K., Verma, R. K., & Pradhan, B. (2026). Integrating CA–Markov–ANN for spatiotemporal prediction of land use dynamics in a fragile Himalayan watershed. *Remote Sensing Applications: Society and Environment*, *41*, 101856. https://doi.org/10.1016/j.rsase.2025.101856

Tilahun, D., Gashu, K., & Shiferaw, G. T. (2022). Effects of Agricultural Land and Urban Expansion on Peri-Urban Forest Degradation and Implications on Sustainable Environmental Management in Southern Ethiopia. *Sustainability*, *14*(24). https://doi.org/10.3390/su142416527

Tilahun, Z. A., Bizuneh, Y. K., & Mekonnen, A. G. (2023). The impacts of climate change on hydrological processes of Gilgel Gibe catchment, southwest Ethiopia. *PLOS ONE*, *18*(6), e0287314. https://doi.org/10.1371/journal.pone.0287314

Tilahun, Z. A., Bizuneh, Y. K., & Mekonnen, A. G. (2024). A spatio-temporal analysis of the magnitude and trend of land use/land cover changes in Gilgel Gibe Catchment, Southwest Ethiopia. *Heliyon*, *10*(2), e24416. https://doi.org/10.1016/j.heliyon.2024.e24416

Toma, M. B., Belete, M. D., & Ulsido, M. D. (2023). Hydrological Components and Sediment Yield Response to Land Use Land Cover Change in The Ajora-Woybo Watershed of Omo-Gibe Basin, Ethiopia. *Air, Soil and Water Research*, *16*(1). https://doi.org/10.1177/11786221221150186

Uddin, M. S., Mahalder, B., & Mahalder, D. (2023). Assessment of Land Use Land Cover Changes and Future Predictions Using CA-ANN Simulation for Gazipur City Corporation, Bangladesh. *Sustainability*, *15*(16). https://doi.org/10.3390/su151612329

Verma, P., Raghubanshi, A., Srivastava, P. K., & Raghubanshi, A. S. (2020). Appraisal of kappa-based metrics and disagreement indices of accuracy assessment for parametric and nonparametric techniques used in LULC classification and change detection. *Modeling Earth Systems and Environment*, *6*(2), 1045–1059. https://doi.org/10.1007/s40808-020-00740-x

Wulder, M. A., Loveland, T. R., Roy, D. P., Crawford, C. J., Masek, J. G., Woodcock, C. E., Allen, R. G., Anderson, M. C., Belward, A. S., Cohen, W. B., Dwyer, J., Erb, A., Gao, F., Griffiths, P., Helder, D., Hermosilla, T., Hipple, J. D., Hostert, P., Hughes, M. J., … Zhu, Z. (2019). Current status of Landsat program, science, and applications. *Remote Sensing of Environment*, *225*, 127–147. https://doi.org/10.1016/j.rse.2019.02.015

Xu, T., Zhou, D., & Li, Y. (2022). Integrating ANNs and Cellular Automata–Markov Chain to Simulate Urban Expansion with Annual Land Use Data. *Land*, *11*(7). https://doi.org/10.3390/land11071074

Yang, L., Driscol, J., Sarigai, S., Wu, Q., Chen, H., & Lippitt, C. D. (2022). Google Earth Engine and Artificial Intelligence (AI): A Comprehensive Review. *Remote Sensing*, *14*(14). https://doi.org/10.3390/rs14143253

Statements & Declarations

Authors contribution

Ermiyas Asfaw Molla: Writing – review & editing, Writing – original draft, Visualization, Validation, Software, Methodology, Investigation, Formal analysis, Data curation, Conceptualization.

Albeza Asfaw Molla: Writing – review & editing, Visualization, Validation, Software, Methodology, Investigation, Formal analysis, Data curation, Conceptualization.

Tilahun Kassa Weldetsadik: Writing – review & editing, Visualization, Validation, Software, Methodology, Investigation, Data curation, Conceptualization.

Zelalem Abera Angello: Writing – review & editing, Visualization, Validation, Software, Methodology, Investigation, Formal analysis, Data curation, Conceptualization.

Robel Fikadu Alemayehu: Writing – review & editing Visualization, Validation, Software, Methodology, Formal analysis, Data curation, Conceptualization

Brook Legese Dhadhe: Writing – review & editing Visualization, Validation, Software, Methodology, Formal analysis, Data curation, Conceptualization

Nahom Bekele Mena: Writing – review & editing Visualization, Validation, Software, Methodology, Formal analysis, Data curation, Conceptualization

Funding

The authors declare that no funds, grants, or other support were received during the preparation of this manuscript.

Competing Interests

The authors have no relevant financial or non-financial interests to disclose.

Ethics, Consent to participate, and consent to publish declarations: Not applicable

Clinical trial number: not applicable.

Data availability

Data generated and analysed during the current study will be made available on request and the authors confirm that all sources are well cited.

Supplementary Files

This is a list of supplementary files associated with this preprint. Click to download.

- ValidationLULC.docx